R. Wenmaekers

The use of microfluidics for the purification of medical radioisotopes

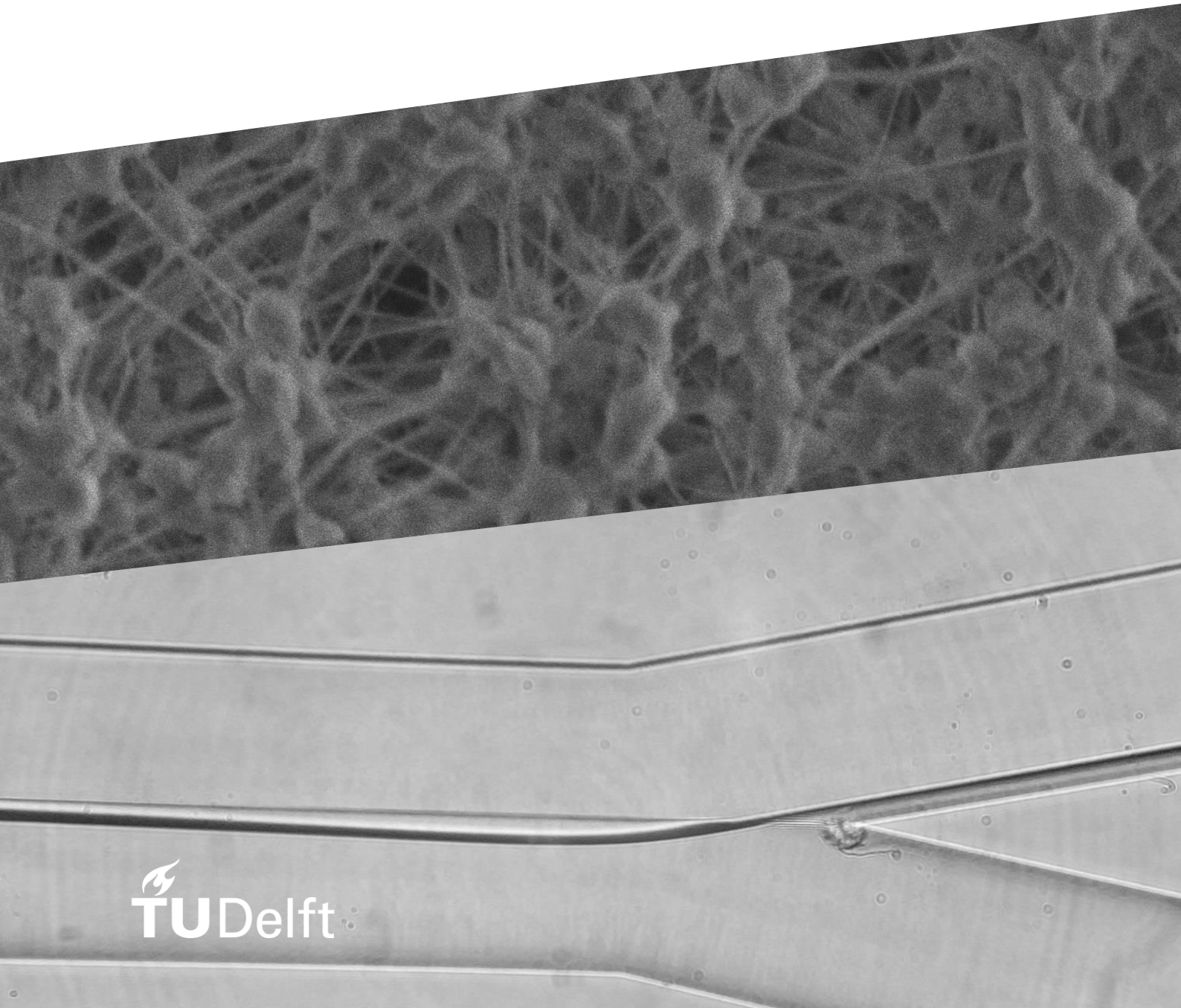

TU Delft

The use of microfluidics for the purification of medical radioisotopes

by

R. Wenmaekers

in partial fulfilment of the requirements for the degree of

Master of Science
in Chemical Engineering

at the Delft University of Technology,
to be defended publicly on April 11th, 2018, at 14:30.

Supervisor:	Prof. dr. E. Oehlke (Elisabeth)	TU Delft
Thesis committee:	Prof. dr. H. Th. Wolterbeek (Bert)	TU Delft
	Prof. dr. E. Oehlke (Elisabeth)	TU Delft
	Dr. P. Serra Crespo (Pablo)	TU Delft
	Dr. H.W. Nugteren (Henk)	TU Delft

TU Delft

Abstract

To obtain radionuclides for medical use from an isotope generator, mother and daughter nuclides need to be separated. In contrast to adsorption-based generators where the mother nuclide is retained on a static column, in liquid generators both mother and daughter nuclides are in solution and need to be separated via extraction. Microfluidic techniques are promising for the extraction process because mass transfer is very efficient and in theory the laminar two-phase flow in the microchannel can be easily separated at the end.

The generator of interest in this thesis is the W-188/Re-188 generator. However, some work also concerns the chemical similar Mo-99/Tc-99m generator and the Lu-177m/Lu-177 generator.

The start objective was to find a less water miscible replacement for the commonly applied organic phase methyl ethyl ketone (MEK) in the W-188/Re-188 generator, since with this system precipitation was observed previously in the microchannel. Several organic phases have been tested for precipitation, but also for their extraction efficiencies and abilities to separate rhenium from tungsten. The best results were observed for 0.2 M Aliquat 336 in 1,3-diisopropylbenzene, an organic phase that shows no precipitation, has suitable wetting behaviour in the microchannel and an even higher extraction efficiency than MEK.

Another issue addressed in this thesis is the incomplete phase separation at the Y-splitter (end) of the channel. Either some aqueous phase leaves through the organic outlet or some organic phase leaves through the aqueous outlet. One possible reason for the leakage is the uniform surface of both outlets, and therefore the preferred wetting of the hydrophilic glass wall of the microchannel with one phase. Coating one side of the microchannel hydrophobically showed that the leakage can be stopped. The effects of radiation on the coating have been investigated using an external gamma source and a threshold of 5 kGy before deterioration was found.

An even easier method to achieve complete phase separation is the use of a membrane separator. Here, two phases are combined in simple 0.5 mm tubing in droplet fashion before being separated by a membrane. With the above mentioned organic phase, an extraction efficiency of 95% was reached within 5.3 minutes contact time. This is considerably longer than the typical contact time in the microchannel (in the order of seconds), but the total handling time was reduced from over 3 hours (with a microchannel) to 16 minutes by using a membrane separator. For lutetium, an extraction efficiency of 99% was reached after 2 minutes contact time, reducing the total handling time by a factor of 2.5 compared to the conventional method.

List of content

Abbreviations and acronyms

β	beta particle
γ	surface tension
γ	gamma photon
θ	(static) contact angle
θ_{adv}	advancing contact angle
θ_{rec}	receding contact angle
μ	dynamic viscosity
$\overline{\nu_e}$	electron antineutrino
ρ	density
ϕ	volumetric flow rate
ϕ	flow rate
A	cross-sectional area
D_h	hydraulic diameter
f_D	Darcy friction factor
h_c	channel height
h_{org}	height ending organic outlet tube
h_{aq}	height ending aqueous outlet tube
n	neutron
p	proton
P	pressure
P	wetted perimeter
Q	flow rate
R	radius
R	count rate
σ	surface tension
v	fluid velocity

CF	Idel'chik correction factor
FP	fission products
FEP	fluorinated ethylene propylene
Gy	Gray
HOR	*Hoger Onderwijs Reactor Delft*, higher education reactor
MEK	methyl ethyl ketone
OTS	octadecyltrichlorosilane
PDMS	polydimethylsiloxane
PEEK	polyether ether ketone
PTFE	polytetrafluoroethylene
SBP	*snelle buizenpost*, fast tube mail system
TBP	tributyl phosphate
TIOA	triisooctylamine
TOA	trioctylamine
TOPO	trioctylphosphine oxide

1 Introduction

Medical radioisotopes for both diagnostic as well as therapeutic purposes are in growing demand worldwide [1]–[3]. They usually have short half-lives so that there is enough time for handling, but the dose to the patient is limited. Most medical radioisotopes are produced in only a dozen nuclear reactors worldwide [4]. Due to the short half-lives and associated issues with transportation, radioisotope generators have been around for decades. These generators allow for the decentral production of short lived isotopes in most parts of the world. The key concept of a radioisotope generator is the separation of the short-lived daughter nuclide from the longer-lived mother nuclide. Most commercial generators use column chromatographic separation [5], but other separation methods are possible such as liquid-liquid extraction.

Microfluidic techniques show a great promise for liquid-liquid extraction due to the large surface-to-volume ratio and the possibility of handling small volumes [6], and have been used extensively in analytics [7]. Work with the technique in the field of radionuclides has mostly been done for the extraction of elements in the actinide group, such as plutonium [8] and americium [9]. The only research done thus far on separating medical radioisotopes by microfluidic liquid-liquid extraction, to our knowledge, has been on the extraction of Cu-64 [10].

The aim of this thesis is to further investigate the possibility of using a microfluidic system – especially a Y-Y microchannel – for the separation of medical radionuclides. The focus lies thereby on the separation of rhenium from tungsten in a W-188/Re-188 generator. Some work was also done on the chemically similar Mo-99/Tc-99m system and on the relatively new Lu-177m/Lu-177 system.

To achieve the goal of this thesis two objectives were addressed:
The first objective is to understand and avoid the formation of precipitate in the microchannel. This phenomenon was observed during previous work on the separation of rhenium from tungsten with methyl ethyl ketone (MEK) in a microchannel [11]. The current assumption in our group is that this is due to the miscibility of MEK and water, however it is not yet known which solvent systems avoid precipitation. The practical outcome of this objective should be to find a less miscible organic phase that can be used in the microfluidic liquid-liquid extraction of rhenium from tungsten. Liquid-liquid extractions in both a conventional setup and a microchannel were performed later in this thesis to test the behaviour and extraction efficiencies of different organic phases.

The second objective – that arose during work on the first objective – is to achieve complete phase separation when using the microfluidic system. In this thesis, the (incomplete) phase separation in a Y-Y microchannel will be described, leakage mechanisms will be proposed, and it will be investigated whether the leakage can be stopped by surface modification of the microchannel with octadecyltrichlorosilane (OTS). The degradation of this OTS coating in an environment with ionizing radiation will also be studied. At the end of this thesis, the use of a membrane separator to obtain complete separation is explored and the effects of radiation on the membrane are investigated.

2 Theory

2.1 Medical radioisotopes

In the decay formulas, the time between brackets behind an equation is the half-life of the nuclide before the arrow and the bold-printed nuclides are stable.

2.1.1 Technetium-99m

Tc-99m is the most commonly used medical radioisotope [4]. It is not used as a treatment (therapeutic), but in diagnostic imaging studies of, among others, the brain, heart, thyroid, lungs, liver, kidneys, bones, blood and tumours [12]. Tc-99m decays mainly by gamma emission, where it emits 140.5 keV gamma rays. These photons can be detected by gamma cameras. Tc-99m has a short half-live of 6 hours, which is very favourable for radiopharmaceutical application, and its decay product Tc-99 has a very long half-live of 211.000 years. Tc-99m is obtained from a generator where it is the decay product of Mo-99.

In generator:	$^{99}Mo \rightarrow {}^{99m}Tc + \beta^- + \overline{\nu_e} + \gamma$	(66 hours)
In patient:	$^{99m}Tc \rightarrow {}^{99}Tc + \gamma$	(6 hours)
	$^{99}Tc \rightarrow \boldsymbol{^{99}Ru} + \beta^- + \overline{\nu_e}$	(211.000 years)

Mo-99 can be produced via various routes, i.e. neutron irradiation of Mo-98 target, proton irradiation of Mo-100 target, or collection from fission products of U-235. High specific activity Mo-99 can only be collected from fission products (FP).

$$^{98}Mo + n \rightarrow {}^{99}Mo + \gamma$$
$$^{100}Mo + p \rightarrow {}^{99}Mo + 2n$$
$$^{235}U + n \rightarrow {}^{99}Mo\ (\sim 6\%) + other\ FP$$

2.1.2 Rhenium-188

Re-188 is a medical radioisotope that is used for therapeutic purposes since it emits a β^- particle. This β^- particle has a maximum energy of 2.12 MeV, which results in an average tissue penetration depth of 3.5 mm [13]. Treatments include bone metastasis, rheumatoid arthritis, intravascular radionuclide therapy and primary cancers [2]. Besides emitting a beta particle, a 155 keV gamma photon is emitted that is suitable for imaging. Rhenium has a relatively short half-live of 17 hours. It decays to Os-188 which is a stable nuclide. Re-188 is obtained from a generator where it is the decay product of W-188.

In generator	$^{188}W \rightarrow {}^{188}Re + \beta^- + \overline{\nu_e} + \gamma$	(70 days)
In patient	$^{188}Re \rightarrow \boldsymbol{^{188}Os} + \beta^- + \overline{\nu_e} + \gamma$	(17 hours)

W-188 is produced by neutron irradiation of W-186 target. Since this route depends on double neutron capture, reactors with a very high neutron flux are necessary to obtain significant amounts of W-188.

$$^{186}W + 2n \rightarrow {}^{188}W + \gamma$$

In this thesis, W-187 is used as a radiotracer since W-188 cannot be produced in our reactor. Because we cannot produce W-188, Re-188 is also not obtained as its decay product. The radioactive rhenium used in this thesis was obtained by neutron activation of rhenium in its natural abundance, producing Re-186 and Re-188.

2.1.3 Lutetium-177

Lu-177 is a promising [3] radionuclide that can be used for therapeutic treatments. Lu-177 decays under emission of a β^- particle to a stable isotope of hafnium. The beta particle has an intermediate energy of 0.13 MeV and the resulting range in tissue is 0.7 mm [13]. This small penetration depth makes this nuclide ideal for the treatment of small primary and metastatic tumours in, among others, the prostate, breasts, lungs and pancreas, for melanoma and for bone palliation therapy [14]. Besides a beta particle, gamma rays are emitted with energies of 113 and 208 keV which allow for simultaneous imaging of the treatment.

In patient: $$^{177}Lu \rightarrow \mathbf{^{177}Hf} + \beta^- + \overline{\nu_e} + \gamma$$ (6.6 days)

Lu-177 can be produced via neutron irradiation of enriched Lu-176, but in this process the nuclear isomer Lu-177m is also formed. It is this isomer, Lu-177m, that is the focus of research in our group as a possible parent nuclide in a generator [15]. Of the Lu-177m, that has a half-life of 160 days, roughly 79% decays to Hf-177 while the remaining 21% decays to the ground state Lu-177 via isomeric transition. The isomeric transition either occurs via the emission of gamma rays, or via internal conversion. With internal conversion, the excess energy of the nucleus is transferred to an inner electron which is ejected from the atom, ultimately causing multiple electrons to be ejected (auger cascade). The ejection of electrons results in a charged state of the atom.

Lu-177m and Lu-177 are chemically and physically similar and differ only in the amount of energy they have. Therefore, they cannot be separated by conventional methods. However, the aforementioned charged state due to internal conversion can be exploited. Lu-177m can be embedded in a complexing agent 1,4,7,10-tetraazacyclododecane-1,4,7,10-tetraacetic acid (DOTA), forming a very stable complex. When Lu-177m decays via internal conversion, the charged state causes bond rupture of the complex which results in un-complexed DOTA and the free (unbound) daughter nuclide Lu-177. This is depicted in equation 2-1. Note that equations 2-1 and 2-2 are simplifications of reality that do not account for charges of the constituents. The complex, indicated as DOTA(Lu-177m), and the now free Lu-177 are chemically different and can be separated by extraction [16].

Bond rupture: $$^{177m}Lu(DOTA) \rightarrow DOTA + {}^{177}Lu$$ 2-1

Dissociation: $$^{177m}Lu(DOTA) \rightarrow DOTA + {}^{177m}Lu$$ 2-2

However, spontaneous dissociation between the Lu-177m and DOTA can also happen. This is depicted in equation 2-2. The spontaneous dissociation is a function of temperature, while the bond nuclear decay (and following bond rupture) is not. Storing complexed DOTA(Lu-177m) at very low temperatures causes a lower and more favourable ratio of free Lu-177m/free Lu-177 [15]. Liquid-liquid extractions, however, need to be performed around room temperature and thus, to minimise the spontaneous dissociation of Lu-177m, handling times at room temperature need to be kept to a minimum.

2.2 Isotope generators

A radioisotope generator produces radionuclides based on the decay of other elements. The generator contains long-lived radionuclides, referred to as the mother nuclide, that decay into short-lived radionuclides of interest, referred to as daughter nuclides. These daughter nuclides build up in the generator and can then be extracted from the generator. Because the mother nuclide has longer half-lives, generators allow for the decentral production – or better, generation – of daughter nuclides. Because of this, radionuclides are available at locations where they otherwise would not be since they would decay during transportation from a central production facility (nuclear reactor or cyclotron). Unlike direct production routes were only part of a target is activated, generators produce no-carrier-added radionuclides (free from stable isotopes).

The most common system is the Mo-99/Tc-99m generator [1]. It usually consists of a column on which the parent nuclide molybdenum-99 is fixed, and from which the technetium-99m is eluted. The elution is sometimes called 'milking' and the generator called a 'cow'. Generators for more than two dozen other radionuclides exist [17], among which the W-188/Re-188 generator studied in this thesis.

It is of great importance that only the daughter nuclide is removed, while the mother nuclide is retained in the generator. Different separation techniques exist, based om different principles. A chromatographic column such as in the Tc-99m generator is the most used separation technique. It exploits the differences in affinity between mother and daughter towards the adsorbent of the column. The major advantage of an eluted column is the simplicity of the system [18].

Examples of other systems are: (i) ion-exchange resins or compounds, (ii) sublimation generators which exploit the differences in temperature where the material becomes volatile, (iii) electrodeposition, where differences in reduction potential are exploited and (iv) solvent extraction, which makes use of the differences in distribution coefficients [5][19]. Solvent extraction, or liquid-liquid extraction is the topic of this thesis.

2.3 Microfluidic system

Microfluidics is a collective name for the handling of fluids, confined on a sub-millimetre scale. There has been a major increase in interest in the field over the past two decades. Microfluidic technologies have countless applications, but most of them are related to chemical and life sciences disciplines. A few examples of applications are: in-vitro diagnostics, high-throughput screening for drug discovery, online process monitoring and detection of threat-posing agents by security forces [7].

The advantages of microfluidic systems, that all follow from the small dimensions, are among others: a high surface-to-volume ratio, small required amounts of sample and little waste production, inherently safer handling of hazardous compounds and integration of multiple stages on a compact (portable) platform [6].

Besides just manipulating less volume, other effects appear as a results of the micrometre scale. Three dimensionless numbers that can be used to express the behaviour of fluids are the Reynolds (Re), capillary (Ca) and Eötvös number (Eo):

$$Re = \frac{\rho v L}{\mu} \qquad Ca = \frac{v\mu}{\sigma} \qquad Eo = \frac{\Delta\rho g L^2}{\sigma}$$

In the above expressions, ρ is the density (kg/m^3), v is characteristic velocity (m/s), L is the characteristic length (m), μ is the dynamic viscosity in (Pa·s), σ is the surface tension in (N/m) and g is the gravitational constant (m/s^2).

The Reynolds number expresses the relative importance of inertia compared to viscosity. Reynolds numbers in microfluidic systems are most often very small and viscous forces dominate. Laminar flow can therefore be expected [20].

The capillary number is a measure for the ratio of viscous forces over surface tension acting across the interface. For very low capillary numbers (Ca << 1), surface or interfacial tensions are dominant, and droplets or bubbles tend to be stable. For large capillary numbers, typically at high speeds, droplets or bubbles deform and can break apart.

The Eötvös number is the ratio of gravitational forces to surface or interfacial tension forces. Low values, typically less than 1, indicate that surface tension is dominant and logically, gravity is no longer the dominant factor.

It is therefore possible – with low Re, Ca and Eo – to have parallel laminar two-phase flow in a microchannel, with the two phases being positioned next to each other instead of on top of each other. The flow behaviour can thus be completely different than the one we are used to at the macroscale.

Microfluidic chips that contain the microchannels can be made from various materials and by various methods [21]. Materials include (borosilicate)glass, silicon, metals, polymers such as PDMS and paper. Manufacturing techniques include etching, machining and moulding, but available techniques depend on the material used. Microfluidic systems can also be distinguished based on the driving force for flow. Flow can be purely capillary driven, pressure driven, or driven by centrifugal, electric or acoustic forces [7]. The microfluidic chips used in this thesis are made from borosilicate glass and the flows are pressure driven.

The design of microfluidic chips can range from a very simple straight channel to extremely complex 3-dimensional structures with valves, reservoirs, mixers and reactors. The type of microchannels used in this thesis is a relatively simple Y-Y channel. It consists of a Y-junction where two inlet channels meet at a sharp angle, a main channel, and a Y-splitter where the main channel is again split into two outlet channels under a sharp angle. A schematic representation of a Y-Y channel is given in figure 2-1. The connected tubing to the chip and the nomenclature used in this thesis is also shown.

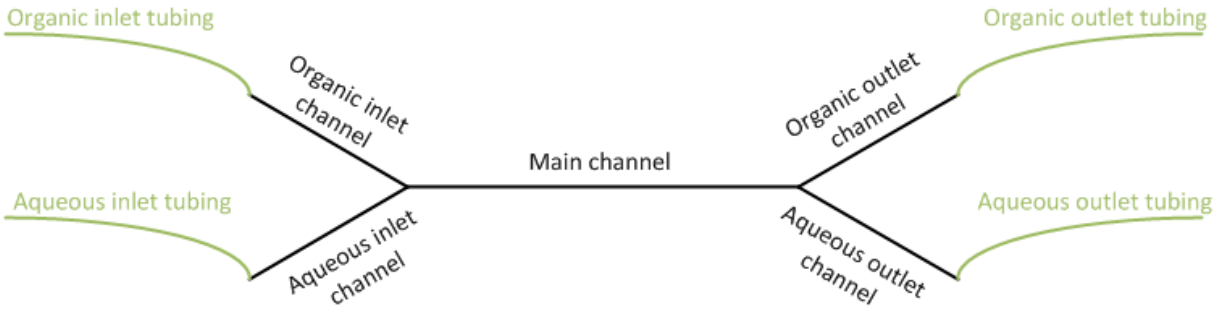

Figure 2-1. Schematic representation of a Y-Y channel (black) plus connected tubing (green), including used nomenclature.

2.3.1 Centred interface

With a two-phase parallel flow, it can be desirable to have the interface at the centre (half-width) of the microchannel. Pohar et al. [22] found an empirical relationship for the flow rate ratio, based on the viscosity ratio, which is required for the interface to be positioned in the middle of the channel:

$$\frac{\Phi_1}{\Phi_2} = \left(\frac{\mu_1}{\mu_2}\right)^{-0.76} \qquad 2\text{-}3$$

2.4 Contact angle

The contact angle is a measure of the wettability of a surface by a liquid. It is the angle at which an interface (liquid-vapour or liquid-liquid) meets a solid. The angle is conventionally measured through the liquid phase, and in case of two liquids through the aqueous phase. The equilibrium contact angle reflects the relative strengths of the molecular interactions between the solid, liquid and vapour or, in case of two liquids, solid and liquids. These molecular interactions are quantified as the interfacial energies (γ). The equilibrium (or static) contact angle is related to the interfacial energies by the Young equation (equation 2-4). The L, V and S in the subscripts stand for liquid, vapour and solid, respectively. The vapour phase might as well be a second immiscible liquid. [23] A schematic representation of a droplet on a surface is given in figure 2-2.

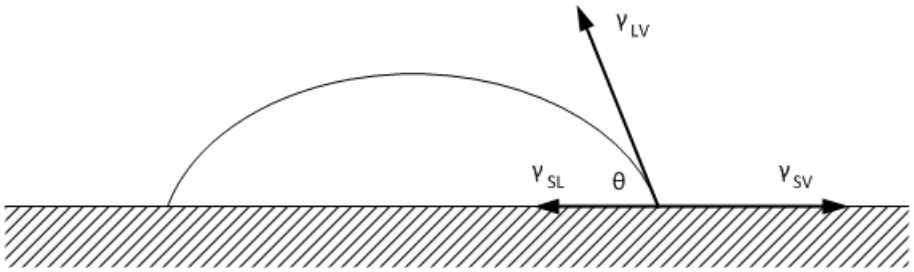

Figure 2-2. Schematic representation of a droplet on a surface, with its contact angle θ and interfacial energies drawn as arrows. The point from which the arrows start is the contact point.

$$\gamma_{LV}\cos(\theta) = \gamma_{SV} - \gamma_{SL} \qquad 2\text{-}4$$

In practice, the contact angle is not always equal to the equilibrium contact angle, but hysteresis occurs. The observed contact angle varies between a maximum value (the advancing contact angle) and a minimum value (the receding contact angle).

When liquid is added to a droplet with an equilibrium contact angle, the contact angle will increase but initially the contact point of the interface with the solid does not move – the droplet stays 'pinned'. Addition of more liquid to the droplet will result in an increase of the contact angle up to the advancing contact angle. When any more liquid is added, the droplet longer pinned stays pinned. The contact point moves (the interface advances) which results in a widened base and a decrease of the contact angle to a new value, below the advancing angle. When removing liquid from a droplet, the contact angle initially decreases until the receding angle while the droplet stays pinned. When any more liquid is removed, the contact point moves (the interface recedes) which results in a shortened base and new contact angle, above the receding angle.

Wetting is another, more qualitative, term to describe the behaviour of a liquid when in contact with a solid. The lower the contact angle of a liquid, the more it wets the solid's surface. In a system with two immiscible liquids, the phase with a contact angle <90° is said to wet the surface. The other

phase is non-wetting. Hydrophilic surfaces are wetted by water while hydrophobic surfaces are wetted by organic phases.

2.5 Surface modification

A surface can be modified to alter the contact angle of liquids on that surface. A surface can be made more hydrophilic or more hydrophobic. Since most surfaces such as metals, ceramics and glass are hydrophilic by nature, a lot of surface modification methods aim at making a surface more hydrophobic. Roughly, two types of surface modification can be distinguished: physical alterations of the surface such as nanopatterning and chemical alterations such as the application of coatings. In this thesis a glass surface is chemically altered through silanization by octadecyltrichlorosilane (OTS).

2.5.1 Silanization

Silanization is the covering of a surface with an organosilane. The organosilane used in this thesis is octadecyltrichlorosilane and will be referred to as 'OTS' or 'silanizing agent'. OTS is a molecule that consists of a silicon atom with three chloride atoms bonded to it, and a long C-18 tail. The chloride atoms react with trace amounts of water and are replaced with hydroxyl groups forming a functional silanol group under divestment of HCl. These silanol groups engage in condensation reactions with the silanol groups present at the surface of the glass substrate, as well as with silanol groups of other OTS molecules, forming covalent silanol bonds. This way, a self-assembled (mono)layer can be formed on the glass surface [24]. A schematic representation of this reaction mechanism is depicted in figure 2-3. The 18-carbon tail gives the covalent coating its hydrophobic nature.

The amount of water plays a crucial role in the formation of the self-assembled monolayer. In the absence of water incomplete monolayers are described to grow, while an excess of water results in polymerization of the OTS [25]. Temperature is also of significance because of the competition between the reaction with a surface silanol group or another OTS molecule. As temperature decreases, the preference for a surface reaction increases and the threshold value is a function of the chain length of the organosilane. For OTS, the threshold temperature below which an ordered monolayer is formed is described to be 18°C [25].

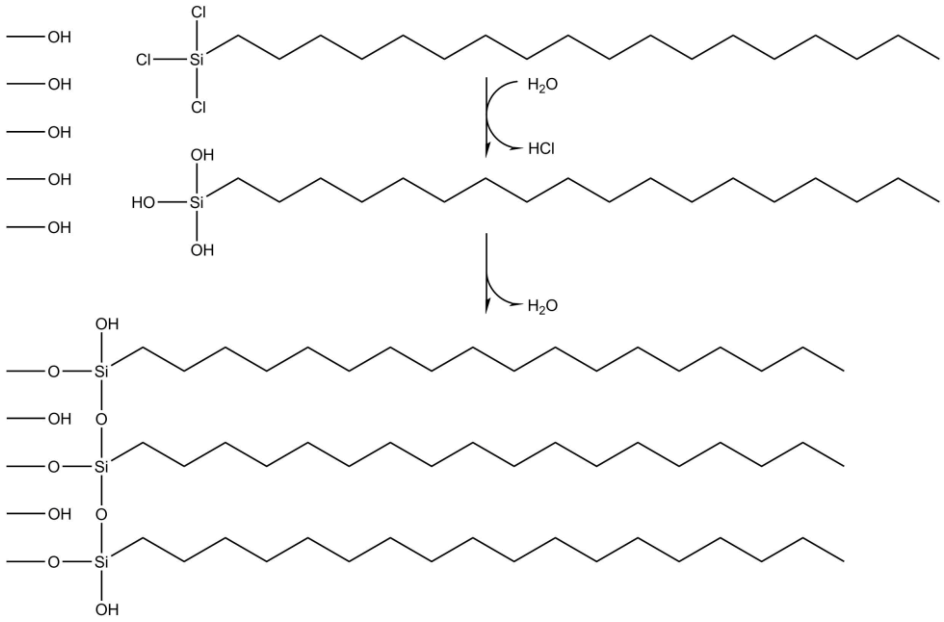

Figure 2-3. Reaction mechanism silanization of hydroxylated surface. -OH groups on the left represent the hydroxylated glass surface.

A weakness of the silanizing agent is the relatively weak C-Si bond. Exposure of a coated surface to UV light through a photomask is a common technique to create patterning on surfaces through cleavage of the C-Si bond [26], [27]. After the cleavage and removal of the 18-carbon tail, a silicon atom is left on the surface and the substrate has grown one atomic layer thicker.

2.6 Liquid-liquid extraction

Liquid-liquid extraction is the method of separating compounds or metal complexes based on their relative solubilities in two different immiscible liquids. The two immiscible liquids are usually an aqueous (polar) phase and an organic (non-polar) phase, but other configurations exist such as an aqueous biphasic system. Liquid-liquid extraction consists of two steps, contact or mixing of the liquids followed by phase separation.

An extraction can be quantified in different ways [28]. The partition coefficient (P) is the ratio of concentrations of an un-ionized solute in two immiscible phases at equilibrium. The distribution coefficient (D) is the ratio of concentrations of all (both ionized and un-ionized) species of the solute. The distribution coefficient D is thus pH dependant. The equations for the partition and distribution coefficient are given in equations 2-5 and 2-6 respectively. The extraction coefficient (E_a°) is an outdated term but it is used in literature that will be referred to in this thesis. The formula as used by Boyd [29] is given in equation 2-7 and relates the activity found in each phase. The extraction coefficient essentially is a distribution coefficient, since measuring the activity does not differentiate between species that the radioactive atom might be part of.

Partition coefficient $$P = \frac{[S]_{org}^{un-ionized}}{[S]_{aq}^{un-ionized}} \quad (2\text{-}5)$$

Distribution coefficient $$D = \frac{[S]_{org}^{un-ionized} + [S]_{org}^{ionized}}{[S]_{aq}^{un-ionized} + [S]_{aq}^{ionized}} = \frac{[S]_{org}^{total}}{[S]_{aq}^{total}} \quad (2\text{-}6)$$

Extraction coefficient $$E_a^\circ = \frac{Activity\ total\ organic\ phase}{Activity\ total\ aqueous\ phase}\left(\frac{V_{aq}}{V_{org}}\right) = \frac{[A]_{org}}{[A]_{aq}} \quad (2\text{-}7)$$

In this thesis, the extraction efficiency is the most used term. It is defined as the percentage of solute moving from one phase to another. For radioactive experiments in this work, it is calculated by dividing the total count rate in the organic phase after the experiment by the total count rate of the aqueous phase before the experiment and multiplying by 100%. Equation 2-7 relates the activities in both phases while we actually measure count rates (in for instance counts per minute). Activity and count rate differ by a factor that is the measuring efficiency of a detector. Although both terms would yield the same result, since we measure count rates it is neater to use count rates in the terms for the extraction efficiency. Count rates are denoted by the letter R.

Extraction efficiency $$EE = \frac{R_{org}^{after}}{R_{aq}^{before}} \cdot 100\% = \frac{R_{org}^{effluent}}{R_{aq}^{feed}} \cdot 100\% \quad (2\text{-}8)$$

The extraction efficiency needs to be calculated with total count rates (as mentioned in equation 2-8). When measurements and calculations yield count rate per volume, [A], the extraction efficiency needs to be corrected for any differences in volume between the two phases. In a continuous extraction in a microchannel, the aqueous and organic flow rates do not have to be equal. When a *ratio* is defined as the flow rate of aqueous phase divided by the flow rate of organic phase, calculations of the extraction efficiency with count rate per volume can be corrected by this ratio, as given in equation 2-9:

Extraction efficiency $$EE = \frac{1}{ratio}\frac{[R]_{org}^{effluent}}{[R]_{aq}^{feed}} \cdot 100\% = \frac{R_{org}^{effluent}}{R_{aq}^{feed}}\frac{V_{aq}}{V_{org}}\frac{100\%}{ratio} = \frac{R_{org}^{effluent}}{R_{aq}^{feed}} \cdot 100\%$$ 2-9

Apart from the extraction efficiency, a 'relative extraction efficiency' is used in this thesis. Instead of relating the total count rate in the organic phase to the total count rate before the start of the experiment, it relates the total count rate in the organic phase to the count rate of the aqueous and organic phase after the experiment, as presented in equation 2-10.

Relative extraction efficiency $$REE = \frac{R_{org}^{after}}{R_{aq}^{after} + R_{org}^{after}} \cdot 100\%$$ 2-10

2.7 Pressure balances

Pressure balances over the microchannel and the membrane separator are described in this section. The pressure balance over the microchannel (and connected tubing) is used as a model in section 4.2.3 'Back pressure loading' of this thesis. It is adopted and paraphrased from Jahromi et al. [30]. The pressure balance over the membrane separator is illustrative for its workings. The balance over the membrane separator is adopted and paraphrased from the paper of Andrea Adamo [31], founder of Zaiput Flow Technologies.

2.7.1 Pressure balance microfluidic chip

A pressure balance [30] is described from the divergence point of the Y-splitter to the end of the aqueous and organic outlet tubing. Different viscosities of the two phases cause different pressure drops in the outlet channels plus tubing, resulting in a pressure difference between the two phases at the Y-splitter. This pressure difference is balanced with the Laplace pressure, originating from the curved interface because one of the phases wets the glass surface.

In the microchannel, the curvature is only in one direction, simplifying the Laplace pressure to:

$$\Delta P_{Laplace} = \gamma\left(\frac{1}{R_1} + \frac{1}{R_2}\right) = \frac{\gamma}{R_1} = \frac{2\gamma cos(\theta)}{h_c}$$ *2-11*

Laplace pressure is a function of the contact angle and can therefore vary between two extremes, given by the advancing and receding contact angle.

$$\frac{2\gamma cos(\theta_{adv})}{h_c} < \Delta P_{Laplace} < \frac{2\gamma cos(\theta_{rec})}{h_c}$$ 2-12

When the pressure difference between the two phases exceeds the possible range of Laplace pressures, the interface is no longer pinned but moves. When the pressure difference is below the minimum Laplace pressure (advancing contact angle), the interface moves towards the aqueous phase. When the pressure difference exceeds the maximum Laplace pressure (receding contact angle), the interface moves towards the organic phase.

To calculate the pressure difference between the two phases, we begin with the pressure loss in the in the outlet channel and outlet tubing. Starting point is the Darcy–Weisbach equation

$$\frac{\Delta P}{L} = \frac{\rho f_D \langle v \rangle^2}{2D_h} \quad \text{2-13}$$

with D_h being the hydraulic diameter (P stands for wetted perimeter) and with f_D being the Farcy friction factor:

$$D_h = \frac{4A}{P} \quad \text{2-14}$$

$$f_D = \frac{64}{Re} = \frac{64\mu}{\rho v D_h} \quad \text{2-15}$$

All experiments are in the laminar flow regime. Rewriting equation 2-13 with the expressions for D_h and f_D results in the following Hagen-Poiseuille equation:

$$\Delta P = \frac{32\mu v L}{{D_h}^2} \quad \text{2-16}$$

$$\Delta P = \frac{32\mu \varphi L}{A{D_h}^2} \quad \text{2-17}$$

or

$$\Delta P = \frac{CF \cdot 128\mu\varphi L}{\pi {D_h}^4} \quad \text{2-18}$$

In equation 2-18 the area A is rewritten as the hydraulic diameter, but because the channel is rectangular instead of cylindrical, the hydraulic diameter and equivalent diameter are not equal. Therefore, Idel'chik introduced a correction factor, here denoted as CF.

The pressure loss between the divergence point of the Y-splitter and the end of the outlet tubing can be written as the sum of the dynamic pressure difference, the pressure loss in the outlet channel and outlet tubing, and the hydrostatic pressure.

$$P_{aq} = P_{dynamic,aq} + P_{loss,aq} + \rho_{aq} g h_{aq} \quad \text{2-19}$$

$$P_{org} = P_{dynamic,org} + P_{loss,org} + \rho_{org} g h_{org} \quad \text{2-201}$$

with the dynamic pressure in the aqueous phase given in equation 2-21 and the pressure loss given in 2-22 as a sum of the loss in the aqueous channel and in the connected aqueous tubing:

$$P_{dynamic,aq} = \rho_{aq} \left(\frac{v_2^2 - v_1^2}{2} \right)_{aq} \quad \text{2-21}$$

$$P_{loss,aq} = \frac{CF \cdot 128\mu_{aq}\varphi_{aq}L_{channel,aq}}{\pi {D_{h,channel}}^4} + \frac{128\mu_{aq}\varphi_{aq}L_{tube,aq}}{\pi {D_{h,tube}}^4} \quad \text{2-22}$$

The dynamic pressure and the loss in channel and tubing are also given for the organic part of the system:

$$P_{dynamic,org} = \rho_{org}\left(\frac{v_2^2 - v_1^2}{2}\right)_{org} \quad \text{2-23}$$

$$P_{loss,org} = \frac{CF \cdot 128\mu_{org}\varphi_{org}L_{channel,org}}{\pi {D_{h,channel}}^4} + \frac{128\mu_{org}\varphi_{org}L_{tube,org}}{\pi {D_{h,tube}}^4} \quad \text{2-24}$$

The pressure loss due to expansion and contraction in the joints between the microfluidic device and the tubing is ignored.

The pressure difference between the two phases at the Y-splitter then is:

$$\Delta P_{phases} = P_{org} - P_{aq} = P_{dynamic,org} - P_{dynamic,aq} + P_{loss,org} - P_{loss,aq} + \rho_{org} g h_{org} - \rho_{aq} g h_{aq} \quad \text{2-25}$$

Or, rewriting the equation to free the organic outlet height:

$$h_{org} = \frac{\Delta P_{phases} + P_{dynamic,org} - P_{dynamic,aq} + P_{loss,org} - P_{loss,aq} - \rho_{aq} g h_{aq}}{\rho_{org} g} \quad \text{2-26}$$

When setting the aqueous outlet height to zero and replacing the ΔP_{phases} with the maximum and minimum Laplace pressures, the maximum and minimum organic outlet heights can be found for which the interface remains in the centre and complete separation should occur, according to the paper of Jahromi et al. [30].

2.7.2 Pressure balance membrane separator

The Zaiput membrane separators working principle is based on a hydrophobic membrane and integrated pressure control component. In this section, a pressure balance [31] over the membrane separator is adopted to clarify the working principles.

The pressure difference over the membrane is defined as $\Delta P_{mem} = P_1 - P_2$ with P_1 on the retentate (non-wetted or aqueous) side of the membrane, and P_2 on the permeate (wetted or organic) side of the membrane.

The pressure loss that arises from the permeate flowing through the membrane is approximated by Hagen-Poiseuille and given by equation 2-27 where μ is the dynamic viscosity, φ the volumetric flow rate, L the pore length, n the number of pores and r the pore radius.

$$P_{per} = \frac{8\mu\varphi L}{n\pi r^4} \quad \text{2-27}$$

P_{per} is the minimum pressure required to drive all the permeate through the membrane when the complete area of the membrane is used. When the pressure over the membrane is greater than P_{per} separation still occurs but less than the entire membrane area is used.

The capillary pressure P_{cap} is a second crucial parameter that must be balanced with other forces in the system to ensure proper separation. The capillary pressure is given in equation 2-28 where γ is the interfacial tension, θ is the contact angle and r is the radius of the membrane pores.

$$P_{cap} = \frac{2\gamma cos(\theta)}{r} \qquad 2\text{-}28$$

There are two modes of failure for the membrane. The first being when the pressure over the membrane is greater than the capillary pressure (P_{mem}>P_{cap}) in which case the retentate breaks through the membrane. The second is when the pressure difference over the membrane is not large enough to overcome the pressure loss indicated by Hagen-Poiseuille (P_{mem}< P_{per}), in which case part of the permeate is retained. Thus, in order to achieve complete separation, the pressure over the membrane must comply with equation 2-29.

$$P_{cap} > P_{mem} > P_{per} \qquad 2\text{-}29$$

The novelty of the Zaiput membrane separator lies in the incorporated pressure control, which is made up of a diaphragm stretched over the retentate stream with the permeate flowing on the opposite side of the diaphragm. The diaphragm seals the retentate flow path such that no flow exists on the retentate side of the membrane as long as P_1 does not exceed P_2 and the additional pressure due to the diaphragm tension P_{dia}.

With $P_1 = P_2 + P_{dia}$ and $\Delta P_{mem} = P_1 - P_2$, it becomes clear that $\Delta P_{mem} = P_{dia}$ and equation 2-29 can be written as follows:

$$P_{cap} > P_{dia} > P_{per} \qquad 2\text{-}30$$

The pressure over the membrane is fixed as being the diaphragm pressure and independent of P_1 or P_2. A proper choice for the diaphragm can thus achieve complete separation.

3
Methods and Materials

3.1 Materials and Instruments

The chemicals used in this thesis and their respective vendors are summed up below. All chemicals are used without further purification or other manipulations unless noted otherwise.

Aliquat 336	Sigma Aldrich
Chloroform	Own stock
Cyclohexane	Sigma Aldrich
1,2-Dichloroethane	Merck
Dichloromethane	Sigma Aldrich
1,3-Diisopropylbenzene	Sigma Aldrich
n-Dodecane	Own stock
Methyl ethyl ketone	Alfa Aesar
MilliQ water	
2-Nonanone	Sigma Aldrich
Octadecyltrichlorosilane, 90+%	Sigma Aldrich
2-Pentanone	Sigma Aldrich
Toluene, dried	Sigma Aldrich
Tributyl phosphate	Sigma Aldrich
Triisooctylamine	Sigma Aldrich
Trioctylamine	Sigma Aldrich

Ammonium perrhenate	Sigma Aldrich
Lutetium chloride hexahydrate	Sigma Aldrich
Methylene blue	J.T. Baker
Sodium molybdate dihydrate	Merck
Sodium tungstate dihydrate	Merck
Water Blue	Merck

The instruments used in this thesis are summed up below.

Centrifuge	SIGMA 113
Contact angle measurer	KSV Instruments, CAM 200
Digital microscope	DNT, DigiMicro Lab5.0 (5-megapixel, 10-500x magnification)
Gamma counter	Perkin Elmer Wallac Wizard
Gamma irradiation chamber	Co-60 GammaCell, doserate: 0.246085 Gy/s on 01-01-2018
Glass cutter	Gamma Bouwmarkt
ICP-OES apparatus	Perkin Elmer, Optima 4300 DV
IMT chip	IMT, ICC-DY15G
Macro cuvette	Helma, 402.000 OG, 20 mm
Membrane separator	Zaiput Flow Technologies, SEP-10
Microfluidic pumps	WPI, Aladdin single-syringe pump
Micronit chip	Micronit, H-microreactor 1.25 microliter
Microscope 1	Bottom viewing, 250x magnification
Microscope 2	AIBOULLY, Top viewing, 45x magnification

Thermoshaker	Grant-bio, PHMT PSC24N
Tubing & connectors IMT	IMT
Tubing & connectors Micronit	IDEX Health & Science
UV light source	UVP Cambridge, UVGL-58 Handheld UV lamp, 254/365 nm, 6 Watt (93mW/cm^2)

3.2 Description of setup, methods and experiments

***IMT* chip**

The *IMT* chip has four ports, two inlet ports and two outlet ports. The chip is fixated in an aluminium holder with four aligned connectors. To the two inlet ports, 25 cm of corresponding tubing (PEEK, I.D. 0.26 mm) was connected and syringe-connectors were attached to the other end of the inlet tubing. Two syringe pumps were used to pump liquids through the inlet tubing into the microchannel. To each outlet port, 25 cm of the same tubing was standardly connected. The behaviour in the microchannel was observed through a microscope that looked from the bottom with magnifications up to 250 times. The microchannel is etched chemically [32] and has a guide structure that runs along the main channel. The main channel is approximately 160 µm wide, 46 µm high and 120 mm long. The exact dimensions are given in Appendix 9.5. A picture of the IMT chip is given in figure 3-1.

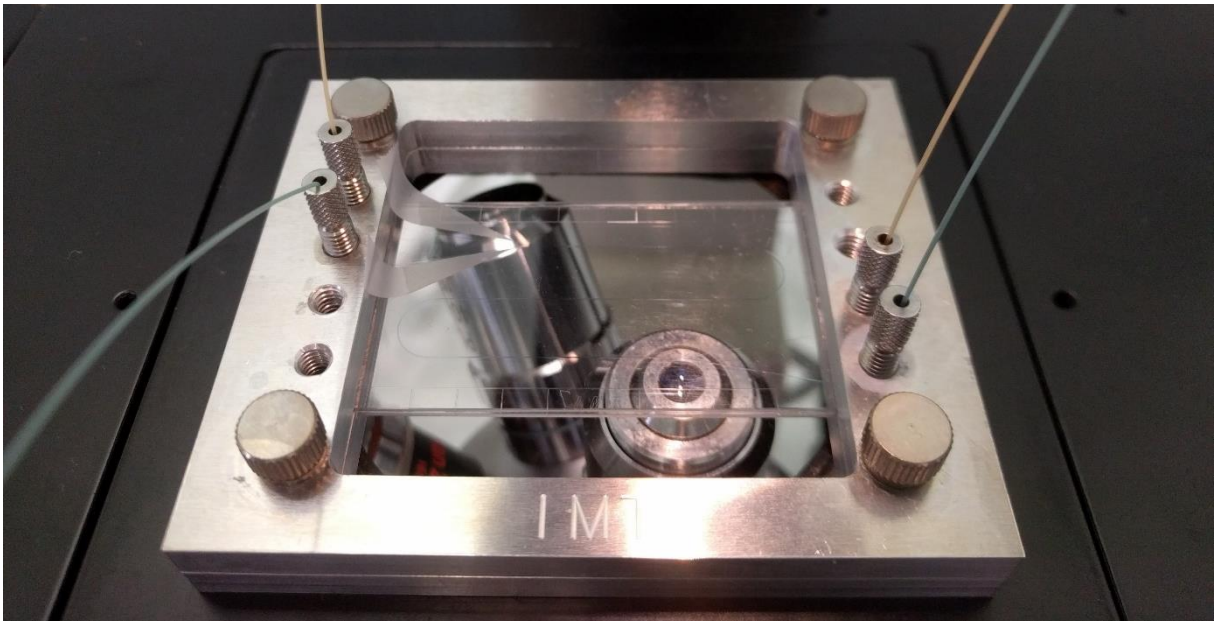

Figure 3-1. Glass IMT chip in its aluminium holder with two inlet and two outlet tubing connected. Microscope looks from the bottom.

***Micronit* chip**

The Micronit chip has four ports, two inlet and two outlet ports. The chip can be easily inserted and removed from an aluminium holder that can be opened with a lever. To the two inlet ports, 25 cm of corresponding tubing (FEP, I.D. 0.51 mm) was connected and syringe connectors were attached to the other end of the tubing. Two syringe pumps were used to pump liquids through the inlet tubing into the microchannel. To each outlet port, 25 cm of the same tubing was standardly connected. Because the microchannel is fabricated by powder blasting [33], the microchannel is not transparent from the bottom. The main channel is 300 µm wide, 150 µm high and the microchannel has a total internal volume of 2.7 µl. The behaviour in the microchannel was observed through a microscope that looked from the top with magnifications up to 45 times.

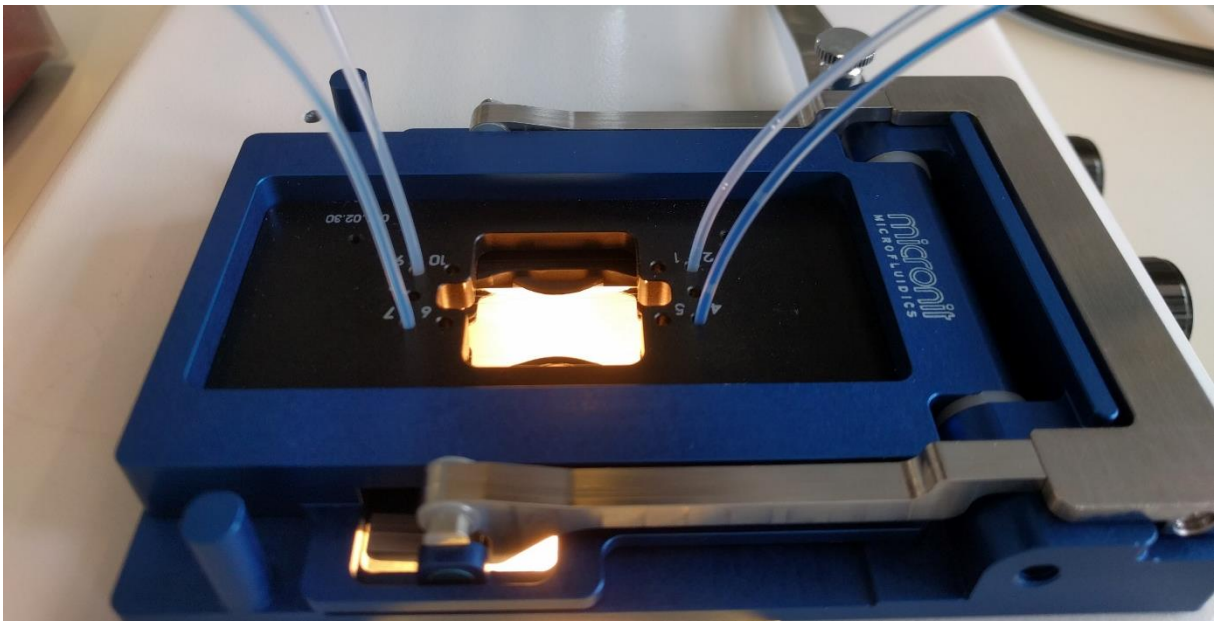

Figure 3-2. Micronit glass chip in its black and blue holder with both inlet and outlet tubing connected. Microscope looks from the top, microchip is lit from the bottom.

Membrane separator

The membrane separator has one inlet and two outlets, one for the organic phase and one for the aqueous phase. The connectors of the membrane separator are compatible with the tubing of the *Micronit* chip. A Y-connector was used to combine the flow from two syringes into one section of tubing that was then connected to the separator's inlet.

- For testing the irradiated membranes, as described later, a 10 cm section of tubing was placed between the Y-connector and the membrane separator.
- For the experiments with coiled tubing, which are described later as well, a 10.5-meter section of tubing was placed between the Y-connector and the membrane separator. This 10.5-meter section of FEP tubing (0.51 mm inner diameter) with a total volume of 2.1 ml was coiled around a glass flask.
  Pictures of the coil are given in section 4.5.3 'Membrane separator behind tubing' in figure 4-21.

Precipitation test

Precipitation tests were done on the *IMT* chip. The aqueous phase feed (solutions of 1-25 mg/ml sodium tungstate dihydrate or 1-25 mg/l sodium molybdate dihydrate in MilliQ water) was normally set to be 20 µl/min and the flow rate of organic phase was adapted to ensure that the interphase was in the middle of the channel. An initial guess for the organic phase feed rate was made with the help of the relation found by Pohar et al. [22] as described in section 2.3 of the Theory. The microchannel was checked for precipitation after minimum 5 minutes (or 200µl) of flow. Pictures were taken with a 12.3-megapixel camera. The microchannel was rinsed with water for at least 5 minutes after each experiment and visually inspected to ensure all precipitate was removed.

Flow behaviour

The flow behaviour of the liquids was tested on the *IMT* chip. The position of the interface was mapped visually by drawings and pictures were taken with a 12.3-megapixel camera.

Membrane irradiation

The PTFE membrane was placed in the centre of the irradiation chamber and irradiated for a period of time, controlled by an automated timer. After irradiation, the membrane's performance was tested by combining 200 µl/min feed flows of both aqueous and organic phase with a Y-connector

before entering the membrane separator. The aqueous feed was coloured with methylene blue (0.1% solution). The effluent was checked visually for breakthrough of aqueous phase (presence of blue droplets in organic outlet). The membrane was dried before each irradiation.

Hydrophobic coating Micronit chip

Before applying the OTS coating, the microchannel had to be completely clean (no fibres present). Since the coating was meant to be applied to the outlet (or Y-splitter), the regular outlet ports were used as inlet ports for the coating procedure. To ensure a hydroxylated surface, the microchannel was rinsed with 1M HCl through both ports at 40 µl/min for 5 minutes. The microchannel was dried with filtered air. Toluene was flown through both ports for approximately 3 minutes at 40 µl/min. It was checked visually that the flow rates of both outlets were approximately equal so that there was no blockage in one of the outlet channels. While keeping the flow of toluene going through the channel that was meant to remain hydrophilic, the other syringe of toluene was replaced with a syringe with the OTS solution. The OTS solution – 2% in dried toluene – was previously prepared in a glovebox. The system was left like this for 20 minutes with both syringe pumps pumping at 40 µl/min. The syringe with the OTS solution was replaced with pure toluene (again, while leaving the other syringe in place) and the system was left with two syringes containing pure toluene for 5 more minutes to ensure all OTS left the microfluidic device, again with both pumps at 40 µl/min. Afterwards, the system was flushed with ethanol at 40 µl/min for 5 minutes to remove all toluene.

Hydrophobic coating glass slides

Glass substrates were obtained by cutting microscope object glasses with a glass cutter to approximately 17 by 17 mm. The glass substrates intended for hydrophobic coating were given a similar treatment as the *Micronit* chip during hydrophobic coating, i.e. they were rinsed with 1M HCl, dried, immersed in a 2% solution of OTS in toluene for 20 minutes and subsequently rinsed with ethanol. After silanization, the samples were rinsed with ethanol and cleaned with a paper towel to remove any excess polymerized OTS. Silanized samples were subjected to UV light as described above.

Removing hydrophobic coating

An attempt to remove the hydrophobic coating was done by exposure of the substrate (*Micronit* chip or glass slide) to long wave UV light (365 nm). The substrates (two glass slides and the *Micronit* chip) were placed on a mirror, about 0.5 cm beneath the UV light source described in the 'instruments' section for periods of time (1-72+ hours).

A second attempt was done by soaking two coated glass slides in a 1M potassium hydroxide solution in methanol (KOH/MeOH) for a period of time (up to one month).

Third, six coated glass slides were placed in the centre of irradiation chamber. With the help of an automated timer, the slides were irradiated for a period of time (1-46 hours), receiving the desired dose (1-40 kGy).

After all removal procedures, contact angles were measured.

Contact angle measurement

Before contact angle measurement, the samples were cleaned with ethanol and handled with disposable powder-free gloves to ensure no dust speckles or other contaminations were present. For static contact angles, a droplet of 5 µl was suspended from the setups pipette tip. The tip was lowered just until the droplet touched the surface and the tip was raised again, leaving the droplet on the surface. A picture was taken and later analysed with the built-in software. For advancing contact angles, the pipette tip was lowered into the middle of a droplet and more liquid was pushed out of the pipette tip. A video was made of the droplet growth and corresponding movement of the interface. Single frames of the video where the interface advances were analysed with the built-in software. For receding contact angles, the droplet was drawn over the surface with the pipette tip and again, single frames were analysed when the interface recedes.

For contact angle measurements in another medium than air, a macro cuvette was used in which the substrate was submersed in the organic phase of choice. All other steps remained the same.

Neutron activation of metals
The target materials for neutron activation were weighted and packed in a PE container. They were inserted in the SBP irradiation facility of the *Hoger Onderwijs Reactor* (TU Delft reactor) with a thermal neutron flux of 1.63E+17 n $s^{-1}m^{-2}$ (and an epithermal neutron flux of 4.66E+15 n $s^{-1}m^{-2}$ and a fast neutron flux of 2.20E+16 n s^{-1} m^{-2}) for a period of time (maximum 15 minutes).

For rhenium, 1 mg of ammonium perrhenate dihydrate was irradiated for 11 minutes. The irradiated material was left standing for three days so that the shorter-lived Re-188 could partially decay, lowering the received dose during consecutive handling. The irradiated material was dissolved in 10 ml aqueous solution to obtain a final solution of 0.1 mg/ml $NH_4ReO_4.2H_2O$, 1 mg/ml $Na_2WO_4.2H_2O$ and 0.01M HCl with a specific activity of 166 kBq ml^{-1} Re-186 and 75 kBq ml^{-1} Re-188 at the moment of solution preparation (72 hours after irradiation).

For tungsten, 1 mg of sodium tungstate dihydrate was irradiated for 7,5 minutes. The irradiated material was left standing for one day so that the shorter-lived Na-24 could partially decay, lowering the received dose during consecutive handling. The irradiated material was dissolved in 10 ml aqueous solution to obtain a final solution of 0.1 mg/ml $NH_4ReO_4.2H_2O$, 1 mg/ml $Na_2WO_4.2H_2O$ and 0.01M HCl with a specific activity of 74 kBq ml^{-1} W-187 at the moment of solution preparation (24 hours after irradiation).

Complete activity calculations are included in Appendix 9.4.

Radioactive conventional extraction
Eppendorf vials (1.5 ml) were numbered and filled with 400 µl of the desired organic phase (all those presented in table 4-1). 400 µl of active aqueous phase was then pipetted into the Eppendorf vials. The vials were shaken in a thermomixer at 1400 rpm for 2 hours at room temperature. Subsequently, the vials were centrifuged at 8000 rpm for 2 minutes to assist phase separation. 200 µl of the top organic phase and 200 µl of the bottom aqueous phase were pipetted out into new Eppendorf vials. Both phases were analysed with γ-counting in the Wallac detector.

Radioactive microfluidic extraction
Extractions were done on the *IMT* chip. Extractions with Re-186 were performed in an acrylic and lead shielded fume hood and the separation at the Y-splitter was monitored with a digital microscope instead of an optical microscope. A mirror was placed beneath the microchip for better visibility of the microchannel through the digital microscope. It was ensured that the microfluidic device and attached tubing were filled with water before the experiment started. The aqueous as well as the organic outlet tubing had a length of 25 cm. Syringes with the active aqueous phase and the desired organic phase were connected to the inlet tubing with a 0.2 µm syringe filter in between. The active syringe was shielded additionally with a sheet of lead. Aqueous flow was established first (typically 20 µl/min), before slowly introducing the organic flow. The organic flow rate depended on the organic phase and its values are given in the Results and Discussion section. Aliquots of approximately 100 µl of the organic outlet flow were taken in pre-weighted 20 ml glass scintillation vials. The first approximately 100 µl after the start of the experiment, or after changing the flow rates was put to waste. The aqueous outlet flow went to a waste vial inside a lead container. A minimum of three aliquots were taken for each set of parameters. The vials were weighed again, and the contents were analysed with γ-counting in the Wallac detector. After use, the microfluidic device was rinsed with ethanol and water (both 40 µl/min, typically for 10 minutes) until no more activity was

measured in the effluent with a handheld Berthold contamination monitor. Figure 3-3 shows a picture of the setup inside the fume hood.

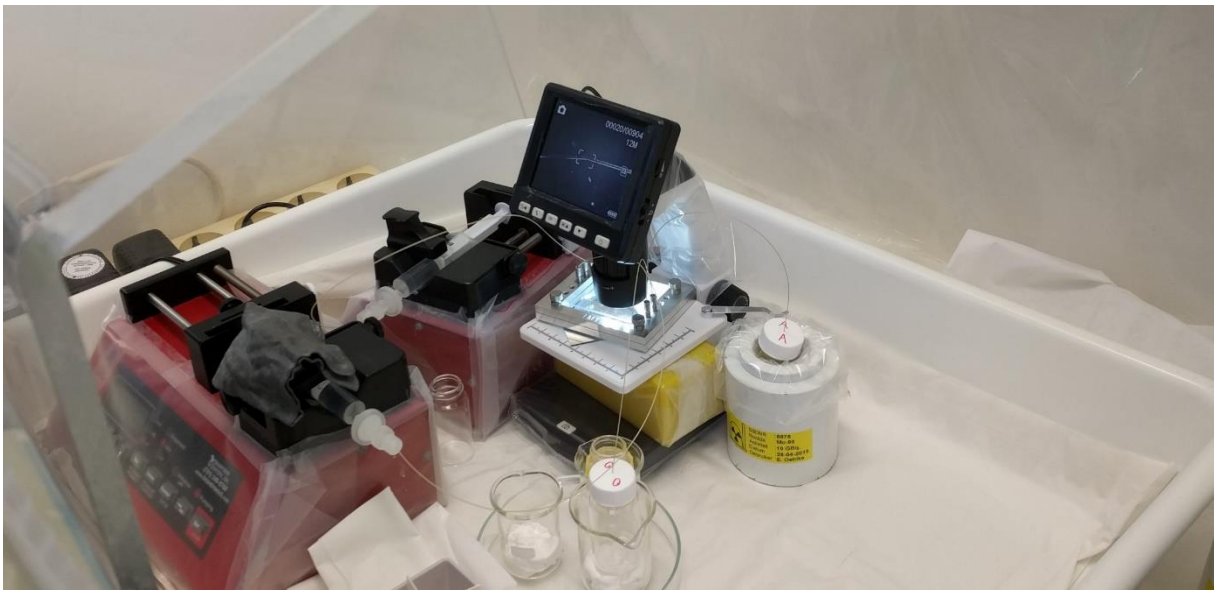

Figure 3-3. Setup for the radioactive extraction on the microchip.

Membrane separator after IMT chip

The organic outlet of the *IMT* chip was blocked by insertion of a piece of plastic between the glass chip and the metal screw connector. The aqueous outlet (now serving as the combined outlet) was connected to the membrane separator with a modified connector. The modified connection was made by screwing an *IMT* syringe connector to a *Luer-Lok* tip with the tubing to the membrane separator fed through the *Luer-Lok* tip. The chip was operated with the same flow rate ratios for the organic liquids that had already been used liquid-liquid extraction in the microchannel without the membrane separator in series, and with a 1:1 ratio for the organic liquids with which no liquid-liquid extractions in the microchannel were performed yet. Roughly 2 ml of aqueous effluent was collected of which 1800 µl was taken out for dilution and subsequent ICP-OES analysis.

Membrane separator after coiled tubing

The coil was rinsed with water before every experiment. During an experiment, the end of the coil was not connected to the separator until all the water had left the coil and the first droplets of organic liquid were eluted. By doing so, the inside of the membrane separator, which was dry before every experiment, only saw aqueous liquid from the experiment and no rinsing fluid. The syringe pumps were set at 200/200, 400/400 and 800/800 µl/min. For the rhenium experiment, the aqueous consisted of 0.1 mg/ml rhenium perrhenate, 1 mg/ml sodium tungstate and 0.01 M HCl and the organic phase was a solution of 0.2M Aliquat-336 in 1,3-diisopropylbenzene. For the lutetium experiment, the aqueous phase consisted of 1 mM $LuCl_3$ in a HAc/NaAc buffer with pH 4.3 and the organic phase was 10% DEHPA in dihexyl ether. More than 1 ml of aqueous effluent from the membrane separator was collected after which 1000 µl was taken out for dilution and subsequent analysis by Induced Coupled Plasma Optical Emission Spectroscopy (ICP-OES).

ICP-OES

Induced Coupled Plasma Optical Emission Spectroscopy (ICP-OES) was used to determine concentrations of rhenium and lutetium in aqueous phases. Samples were diluted with 1% HNO_3 until a maximum concentration of 10 mg/l. A calibration line (0, 2, 4, 6, 8 and 10 mg/l) was made with ICP standard solutions of rhenium and lutetium.

4

Results and Discussion

4.1 Precipitation

Previous work done in our group by Ilza Dalmázio [11] has shown that precipitation can happen in the microchannel when extracting medical isotopes. An example is the extraction of rhenium with methyl ethyl ketone (MEK) from an aqueous solution containing both rhenium and tungsten. Growth of a precipitate in the microchannel can disrupt the laminar flow of the solvents, a precipitate shot loose can block an outlet channel, or the precipitation may eventually clog the microchannel entirely.

The precipitation mechanism is not clear. MEK and water are partly miscible. The current explanation in our group is that at the interface (which is not sharply defined with miscible liquids) a third transition phase occurs. The solubility of the metal salts in this transition phase is less than in the bulk phases which can lead to precipitation.

To investigate if replacing MEK with a solvent that is less miscible with water avoids precipitation, several solvents and extractants were selected based on suitability to extract technetium or its homologue rhenium as mentioned in literature [19], [29], [34]–[38], low water solubility, relatively low toxicity, availability and pricing, and chemical (dis)similarity with other chosen solvents. In total, nine different solvents and four extracting agents were selected and were tested in different combinations, as detailed in table 4-1.

The different organic phases (given in the first column of the table) were pushed through the *IMT* chip together with an aqueous solution of sodium tungstate or sodium molybdate, and the microchannel was checked for precipitation.

The solvents are ordered in table 4-1 on decreasing solubility in water. Dark boxes indicate precipitation, light boxes indicate minor precipitation and a hyphen indicates that no precipitation was visible at all. The distinction between the light and dark boxes is subjective but in the absence of a quantitative characterisation, this method was chosen. A precipitate indicated by a light box is not thought to disrupt the laminar flow or affect the microchips performance in any other way, at least not for the duration of the experiment (complete emptying of a 5 ml syringe, which takes roughly 2 hours). Some boxes are left empty. When there was no precipitation observed at the highest concentration, it was assumed that precipitation also would not happen at lower concentrations and thus these experiments were not conducted.

Pictures of the typical precipitate can be found in figure 4-1. Appendix 9.1 holds a complete series of pictures for all results presented in table 4-1. The precipitation always happened in the organic phase, and it grew to the glass wall.

For pure solvents, precipitation was observed in 2-pentanone, tributyl phosphate and 2-nonanone for both sodium tungstate and sodium molybdate, and in dichloromethane for only sodium tungstate. Minor precipitation was observed in 1,2-dichloroethane and chloroform for sodium tungstate only. With the extractant solutions, minor precipitation was observed in E06 (TOPO in dichloromethane) for sodium tungstate only.

solvent	*solubility in water (%)*		*0.1% W*	*0.5% W*	*1% W*	*2.5% W*	*0.1% Mo*	*0.5% Mo*	*1% Mo*	*2.5% Mo*
2-pentanone	6	[39]								
dichloromethane (CH_2Cl_2)	1.3	[40]	-	-			-	-	-	-
1,2-dichloroethane	0.9	[41]	-	-			-	-	-	-
chloroform ($CHCl_3$)	0.8	[42]	-	-			-	-	-	-
tributyl phosphate (TBP)	0.6	[43]	-				-			
2-nonanone	0.04	[44]	-				-			
cyclohexane	0.006	[45]	-			-	-			-
1,3-diisopropylbenzene	0.004	[46]	-			-	-			-
n-dodecane	0.000	[47]	-			-	-			-
30%TBP, 16%TOA in cyclohexane (E01)			-	-	-	-				-
30%TBP, 16% TOA in n-dodecane (E02)						-				-
0.2M Aliquat 336 in 1,3-diisopropylbenzene (E03)						-				-
0.2M Aliquat 336 in 2-nonanone (E04)						-				-
0.1M TOPO in cyclohexane (E05)						-				-
0.01M TOPO in dichloromethane (E06)										-
0.1M TIOA in cyclohexane (E07)						-				-

Table 4-1. Precipitation for various solvents and extractant solutions in combination with aqueous solutions of molybdate and tungstate. 'W' means sodium tungstate dihydrate and 'Mo' means sodium molybdate dihydrate, percentages are mass/volume-percentages %(w/v). Light blue boxes indicate minor precipitation, dark blue boxes indicate precipitation and hyphens indicate no visible precipitation.

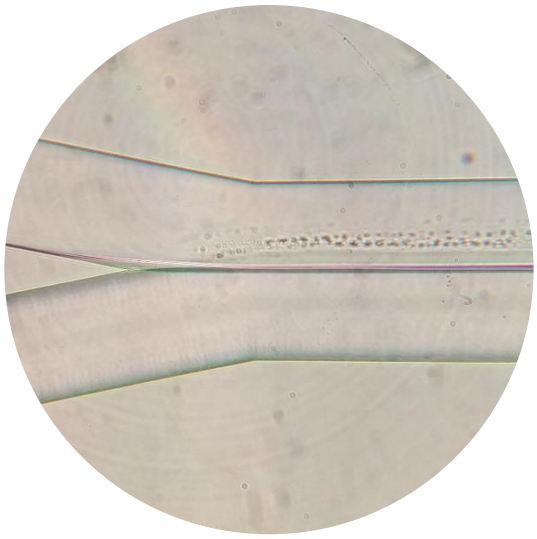

Figure 4-1. Precipitation in the microchannel at the organic side of the interface. Aqueous phase contains 1% Na_2WO_4 and organic phase is 2-nonanone. Top phase is the organic phase, bottom phase is the aqueous phase[1].

The solvents in which most precipitation happens are 2-pentanone, 2-nonanone and tributyl phosphate. These three compounds each have a functional group with two free electron pairs on an oxygen atom that can interact with the tungstate or molybdate.

When we compare 2-pentanone and 2-nonanone – both methyl ketones but with different length hydrocarbon chain – precipitation in 2-nonanone starts at higher concentration. This might be a result of the lower water solubility of 2-nonanone (0.04%) compared to 2-pentanone (6%). When we ignore the precipitation in TBP and 2-nonanone (which might be more profound due to interactions of the oxo group), it is observed that precipitation decreases with decreasing water solubility. The fact that the only minor precipitation in the extractant solutions happens in E06 where the solvent is dichloromethane (most water-soluble solvent) further backs the possibility that water solubility plays a role.

Furthermore, precipitation is more likely to happen with tungstate than with molybdate. This is especially clear with dichloromethane, 1,2-dichloroethane, chloroform and E06 where (minor) precipitation happens with tungstate while no precipitation is present with molybdate.

Thus, three trends may be distinguished:

i. Precipitation happens more in solvents with an oxo group
ii. Precipitation decreases with decreasing solvent solubility in water
iii. Precipitation is more likely to happen with tungstate than with molybdate

The precipitation experiments were carried out with tungsten and molybdenum and not with rhenium and technetium, which would also be present in an actual generator. In Dalmázios experiments with MEK where precipitation happened, rhenium was also present in the aqueous phase. However, the concentration of tungsten in these experiments was more than ten times greater than rhenium and it is assumed that tungsten is responsible for the precipitation instead of rhenium.

[1] Unless noted otherwise, in all pictures and figures in this thesis the top phase is the organic phase, and the bottom phase is the aqueous phase. Although interfacial forces dominate gravitational forces on this scale and the pictures and figures are a top view (the microchip is lying flat), the fact that organic liquids usually (at least the ones used in this thesis) float on aqueous liquids is a useful mnemonic.

Another possible cause for the precipitation is the formation of hydroxide complexes (polymers) which, at a certain pH, molybdate and tungstate are known to form. All aqueous solutions used for the precipitate experiments were made with MilliQ water, without any addition of buffer, acids or bases. The pH of the solutions was measured, and the speciation was calculated with *CHEAQS Next* software [48]. The results are presented in table 4-2.

Aqueous phase	pH	MoO_4^{2-} (%)	$HMoO_4^-$ (%)
0.1% $Na_2MoO_4 \cdot 2H_20$	6.30	99.28	0.71
2.5% $Na_2MoO_4 \cdot 2H_20$	8.21	99.99	0.01

Aqueous phase	pH	WO_4^{2-} (%)	HWO_4^- (%)
0.1% $Na_2WO_4 \cdot 2H_20$	6.58	99.91	0.09
2.5% $Na_2WO_4 \cdot 2H_20$	8.28	100	0

Table 4-2. Calculation of speciation with CHEAQS Next based on measured pH values. 'Mo' stands for sodium molybdate dihydrate, 'W' stands for sodium tungstate dihydrate and percentages in the left column are weight/volume-percentages %(w/v).

Less than 1% of the molybdenum or tungsten species are in the monohydrated form, and with increased concentrations this number drops to practically zero. Species with more than one protonation were not calculated to be present. At the measured pH values, molybdenum and tungsten exist almost purely as molybdate or tungstate and should not form polymers which could lead to precipitation.

It is not impossible to isolate the precipitate from the microchannel to conduct further research on its chemical composition. Although a few observations were made, the exact mechanism of precipitation remains unclear. However, this is not crucial for this project. Or, to quote Baes from his book The Hydrolysis of Cations [49]:

> *''In many separation processes involving precipitation, ion exchange, or solvent extraction, while a knowledge of the hydroxide complexes formed by the metal ion would be desirable, it is often not essential to successful application.''*

4.2 Interface challenges

4.2.1 Aqueous leakage

One of the first observations during the precipitation experiments on the *IMT* chip was the leakage of the aqueous phase at the Y-splitter into the organic outlet. The interface does not stop at the sharp point of the Y-splitter but runs off through the organic outlet. Figures 4-2a and 4-2b depict the Y-junction and Y-splitter of the *IMT* microchannel, respectively. In figure 4-2b, the interface can be seen running of through the organic outlet.

The leakage of the aqueous phase into the organic outlet is a phenomenon that was observed at all flow rates for all pure solvents tested for the extraction of rhenium (see table 4-1) and for the extraction of lutetium with an organic phase of 10% DEHPA in dihexyl ether (for details see section 4.5.3). If the interface runs along the middle of the microchannel, or even slightly below the middle, at the Y-splitter the interface will still leave through the top (organic) outlet.

The aqueous and organic feeds were switched so that the aqueous phase was fed from the top, but also in this case there was still leakage of the aqueous phase to the organic outlet. The feed

configuration does, therefore, not affect the separation behaviour. This was expected since the microchip was lying flat and the microchannel is symmetrical. All further experiments were done with the organic phase on 'top'.

The probable reason for the observed leakage is that the hydrophilic glass microchannel is wetted preferably by the aqueous phase. There is, however, surprisingly little literature on this aqueous leakage phenomenon. Huh et al. mentioned the problem, but then concentrated on solving the problem by applying a hydrophobic coating to the glass [50].

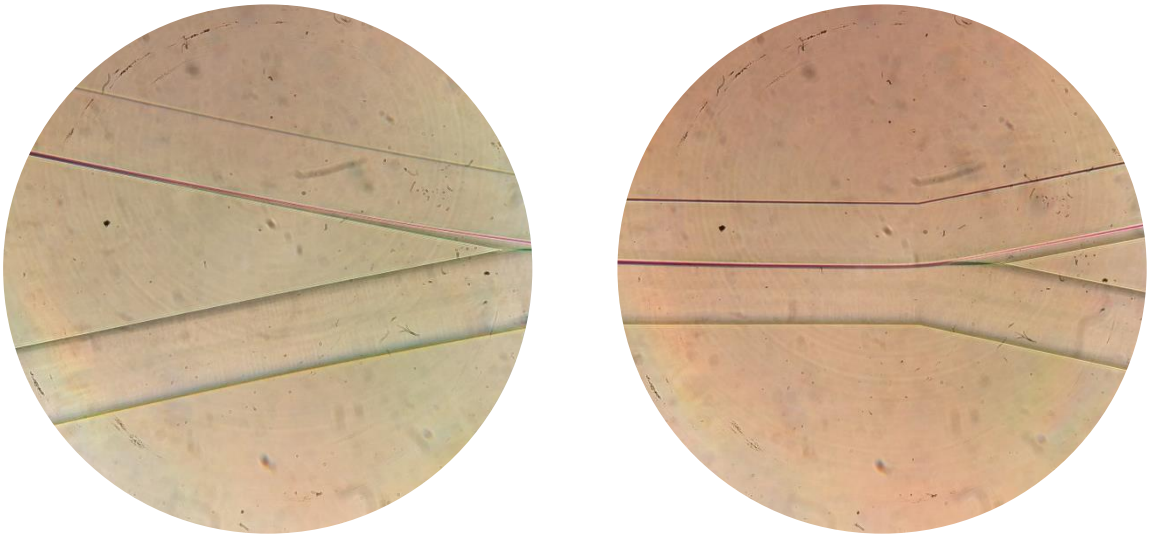

Figure 4-2. a) Aqueous infiltration at the inlet (left) and b) aqueous leakage at the outlet (right).

Similar behaviour was observed at the inlet. The glass is again favourably wetted by the aqueous phase and the aqueous phase is drawn into the organic inlet channel. Unlike at the exit, the organic phase flows in the opposite direction to the invading aqueous phase and the resulting shear forces stop the further invasion of the aqueous phase. The result is a displacement of the start of the interface of only a few millimeters stream upwards of the organic inlet. The aqueous infiltration is depicted in figure 4-2a.

Varying the flow rates (while keeping the flow rate ratio constant) shows that the interface invades the organic inlet more when the flow rates decrease. This makes perfect sense as the shear stress is a function of the velocity gradients at the interface while the interfacial energies between the glass and the aqueous phase are material properties and not dependant on flow rates. The infiltration as a function of flow rates is depicted in figure 4-3.

This aqueous infiltration at the inlet is not really a problem for our purposes. It was merely observed that at very small flow rates (below 5µl/min aqueous phase), the invasion of aqueous phase 'pinched off' the organic inlet, disrupting the steady state laminar flow. At high flow rates, the invasion is negligible.

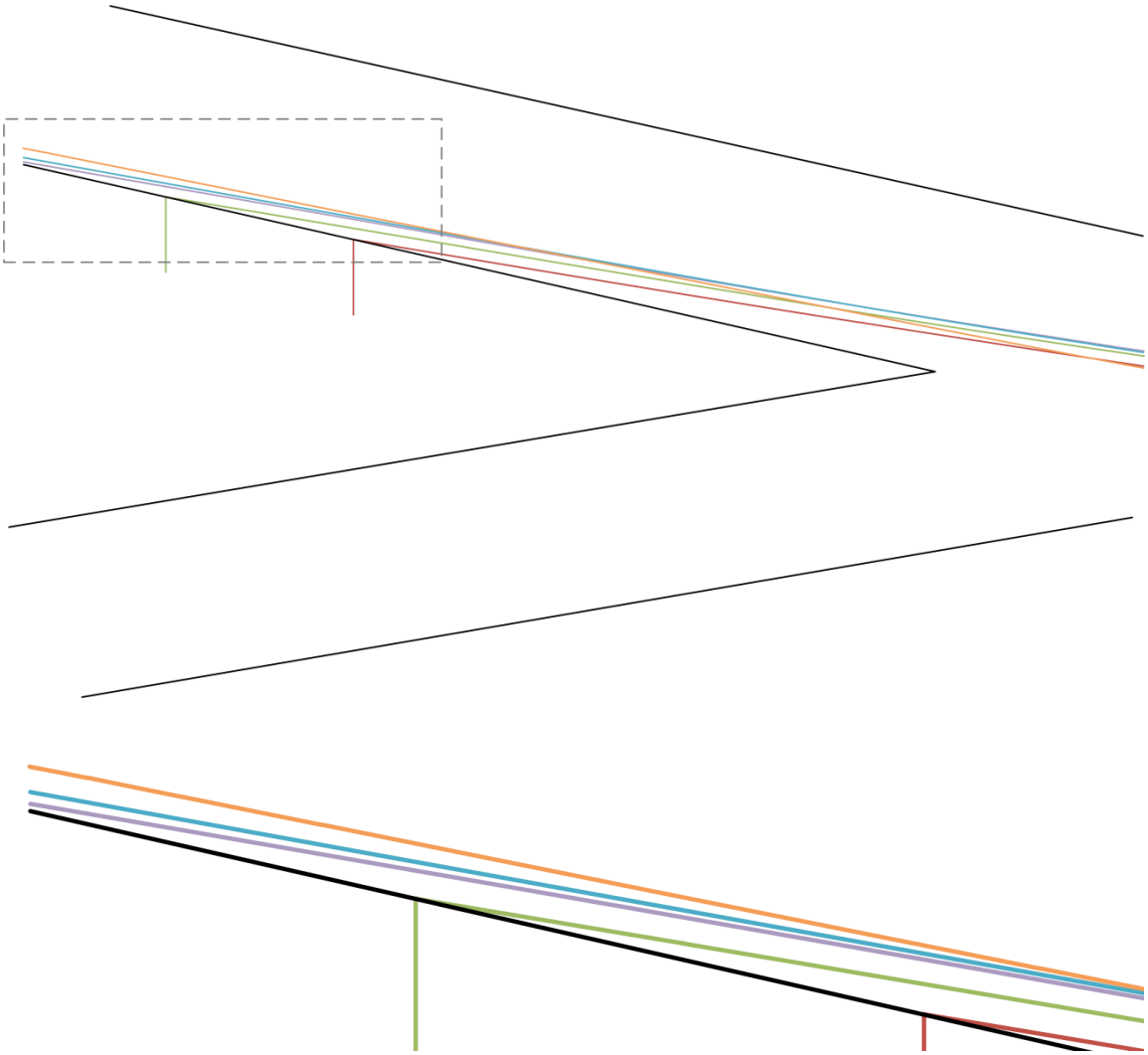

Figure 4-3. Infiltration of aqueous phase in the organic inlet channel. Top: overview of the Y-junction. Bottom: enlarged area within the dashed box. Aqueous phase flow rates 40 µl/min (red), 20 µl/min (green), 10 µl/min (purple), 5 µl/min (blue) and 2.5 µl/min (orange), organic phase is cyclohexane (x 1.08). Figure is made in Visio by drawing lines over actual photographs, which can be found in Appendix 9.2.

4.2.2 Simultaneous aqueous and organic leakage

The flow rate ratio between the aqueous and organic phase – which was previously set so that the interface was positioned in the middle of the channel – was altered to displace the interface towards the aqueous side of the channel in the hope that the interface would leave through the aqueous outlet. This way, the aqueous effluent would be contaminated with some organic phase, but the organic outlet would be pure. A pure organic phase is necessary with the nuclide generator application in mind, because contamination of the daughter isotope rhenium (which is in the organic phase) with tungsten (which is in the aqueous phase) is unacceptable for patient doses.

However, a pure organic phase was not observed, but simultaneous to the leakage of the aqueous phase into the organic outlet, the organic phase left through the aqueous outlet. This was observed by looking at the outlet tubing. The aqueous phase was dyed with methylene blue for clarity and blue liquid could be seen passing through the organic outlet tube. At the same time, colourless liquid could be seen passing through the normally blue aqueous outlet tube. Looking through the microscope, this was not clear though. No more than a smudge could be observed by eye due to very fast interchange of different states. Frame by frame examination of a recording with a relatively high

framerate of 120 fps while keeping the flow rates low (aqueous flow rate 5 µl/min) gave a better insight into the leakage of the organic phase.

A displacement of the interface from the middle towards the aqueous side was not (completely) stable. The displaced interface would be stable for some time and distance into the microchannel but would then become unstable and vary between two states. It was not possible to determine the start of the instability exactly because the microscope did not give a complete overview of the entire microchip. However, we had the impression that the instability travels backwards in the opposite direction to the flow. In figure 4-4, the situation is sketched showing the case where the instability starts already at the Y-junction. The interface moves between the two dashed lines.

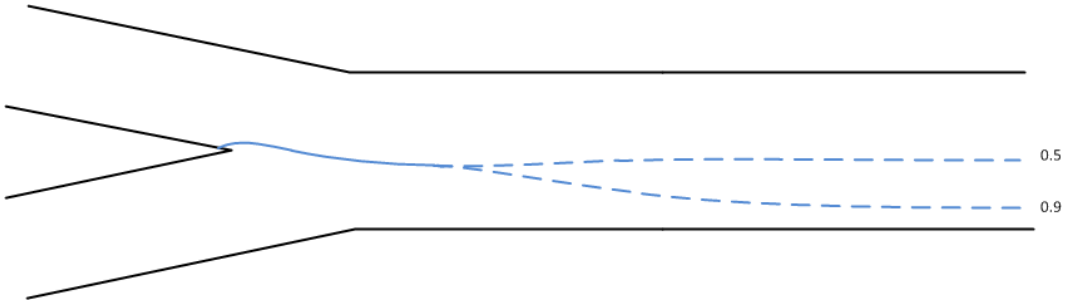

Figure 4-4. Interface instability at the inlet. Interface alternates between the two dashed lines. If the top wall is considered to be at position 0 and the bottom wall at position 1, the dashed blue line in the middle is at position 0.5 and the bottom dashed blue line is considered at position 0.9 for ease of explanation.

It is not entirely clear why a displacement of the interface from the middle to the aqueous side is not stable. What is observed, is that the interface position varies between the middle of the channel (0.5) and an extreme position (0.9), depending on the flow rates used. The cause of this phenomena could be that the interface 'snaps' back to the guide structure in the middle of the channel. The favourable position at the guide structure might be explained with the use of the contact angle.

The surface of the microchannel is flat near the walls of the channels with a guide structure in the middle of the channel. The slope of the guide increases towards the centre where it is highest. A schematic representation of the guide structure (black) and organic-aqueous interface (blue) is given in figure 4-5. The position at 0.7 is found to be not stable. When the pressure on the (right) aqueous side increases, the contact angle will increase up to the point where it is equal to the advancing contact angle. Any further increase will result in a movement of the interface (or specifically its contact point with the surface) to the left. On a flat surface this results in new contact angle which is smaller than the advancing contact angle and a new equilibrium position is reached. On the guide structure however, a movement of the contact point to the left results in an increase of the contact angle because the slope of the surface increases. This increase of the contact angle is visible when comparing the angles at points 0.7 and 0.5 in figure 4-5. It is possible that the decrease in contact angle, resulting from the base of the aqueous phase becoming wider, is overcompensated by the increase in contact angle resulting from the increasing slope. Since the new value of the contact angle does not become smaller than the advancing contact angle, the interface moves all the way to the top of the guide.

When the pressure on the (left) organic side increases, the opposite can happen. The contact angle will decrease up to the receding value. When it becomes smaller than the receding contact angle, the contact point moves to the right. Because the slope decreases, the contact angle also decreases upon movement to the right. This decrease in the contact angle is visible when comparing points 0.7 and 0.9 in figure 4-5. It is possible that the increase in contact angle, resulting from the base of the aqueous phase becoming smaller, is overcompensated by the decrease in contact angle resulting

from the decreasing slope. Since the new value of the contact angle does not become bigger than the receding contact angle, the interface moves off the guide structure up until the flat part.

Thus, instead of a stable displaced interface position at for example 0.7, the interface fluctuates rapidly between the guide structure at 0.5 and the extreme at 0.9 to maintain the 0.7 average as given by the flow rates.

Since the guide structure is suspected of influencing the interface position, it would be interesting to experiment with different guide configurations, or for that matter with completely different splitters. The manufacturing of such microchannels in polydimethylsiloxane (PDMS) was considered, but PDMS was not compatible with the used solvents [51].

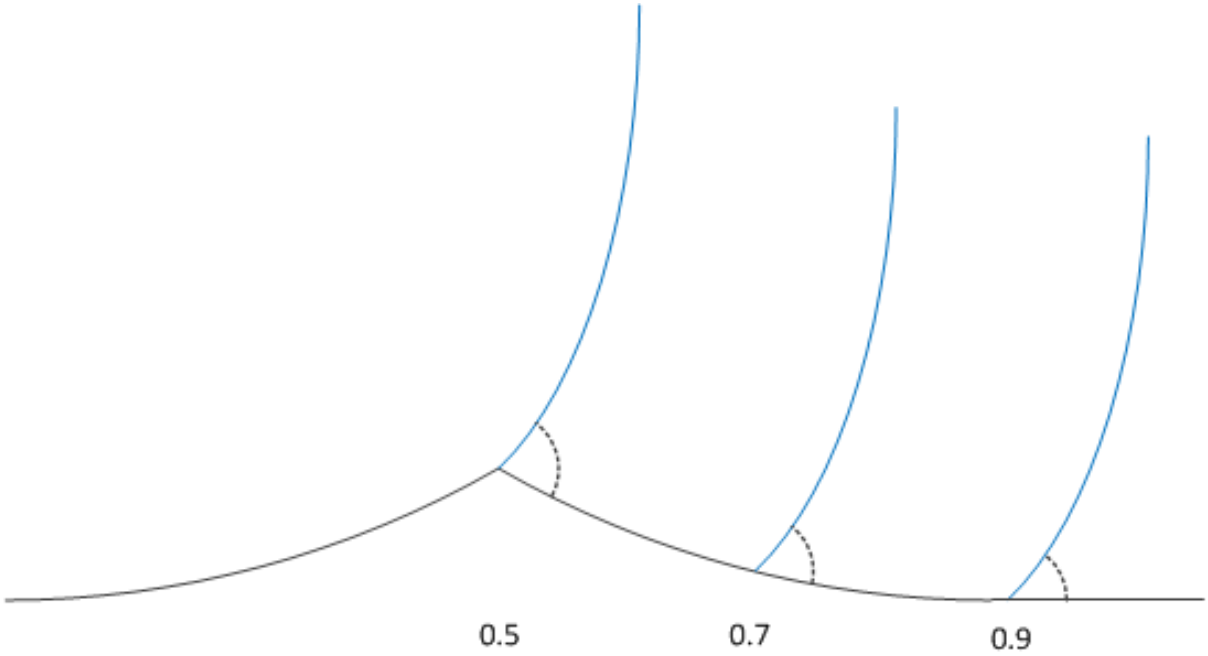

Figure 4-5. Schematic of contact angle interaction with guide structure, cross-sectional view. Interface is depicted by the three (identical) blue lines. Organic phase is on the left of the blue line, aqueous phase on the right. Contact angle at 0.5 > contact angle at 0.7 > contact angle at 0.9.

Because of this fluctuation of the interface position, a transient flow reaches the Y-splitter at the end of the microchannel. The resulting behaviour is sketched in figures 4-6 to 4-8 over actual stills from the video using Visio. It must be noted that these sketches are not stills from consecutive frames of a single event. Instead, several relatively sharp frames were selected, and the event was reconstructed. The frames from which the drawings were made can be found in Appendix 9.3.

In the first series of figures can be seen that a large section of organic liquid reached the Y-splitter. The Y-splitter is wetted with an aqueous film and remains wetted by the aqueous phase as a wide section of organic phase reaches the Y-splitter. Two possibilities are observed:

1. The interface remains intact and there is no leakage of organic phase through the aqueous outlet (sketched in figures 4-6).
2. The interface breaks and a droplet of organic phase leaves through the aqueous outlet (sketched in figures 4-7 and 4-8).

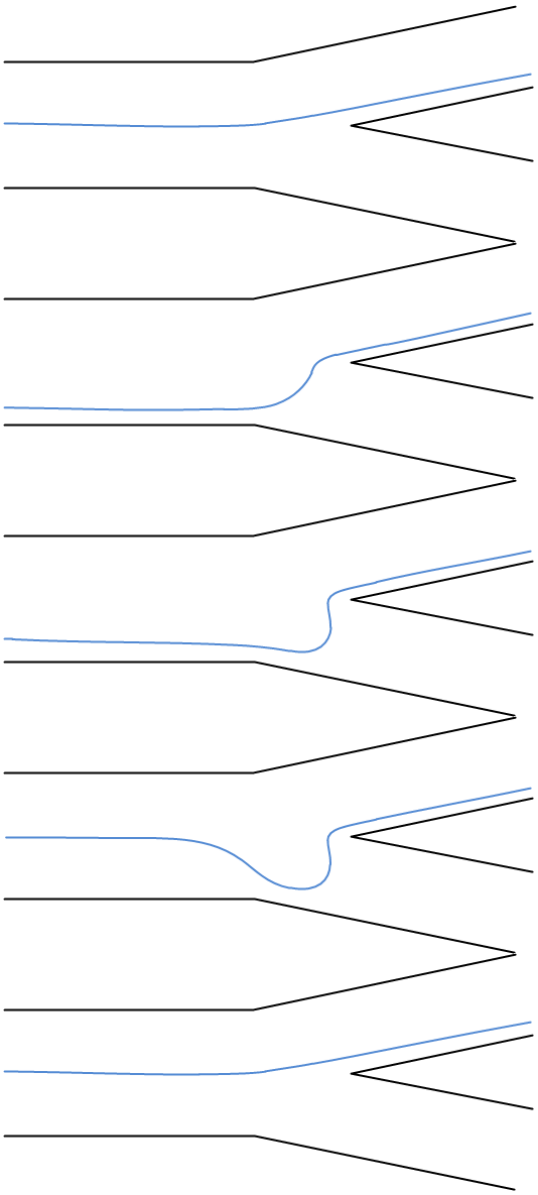

Figure 4-6 a) to e) from top to bottom. Interface remains intact.

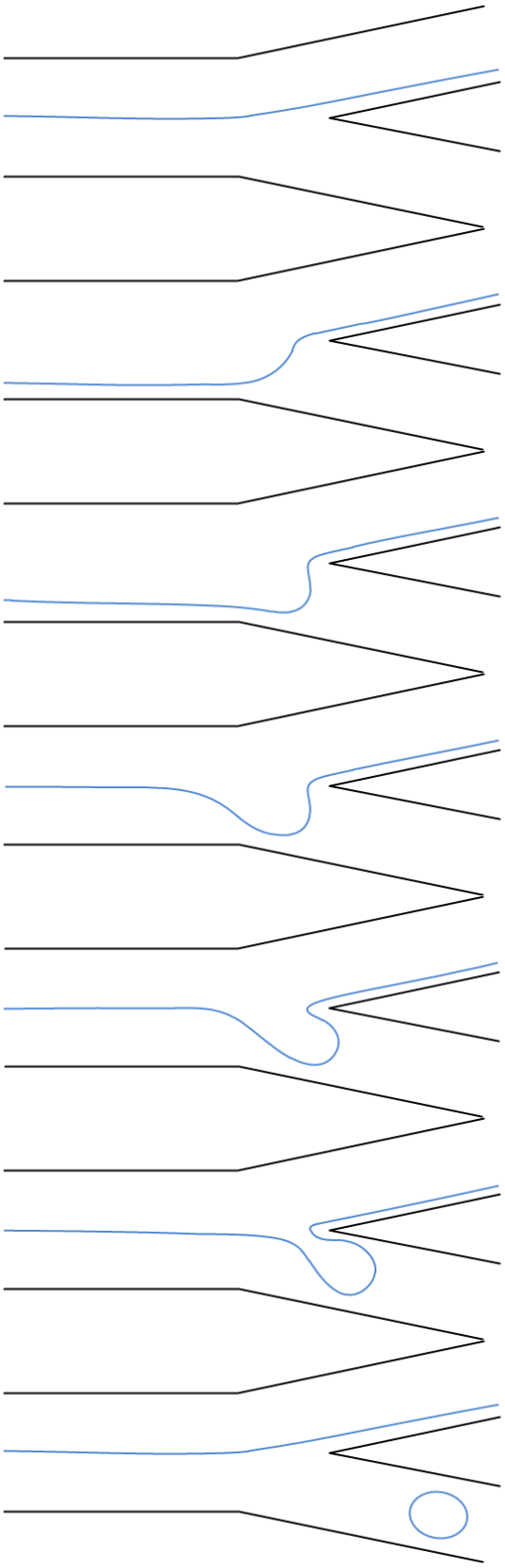

Figure 4-7 a) to g) from top to bottom. Interface breaks and a droplet of organic liquid leaves through the aqueous outlet.

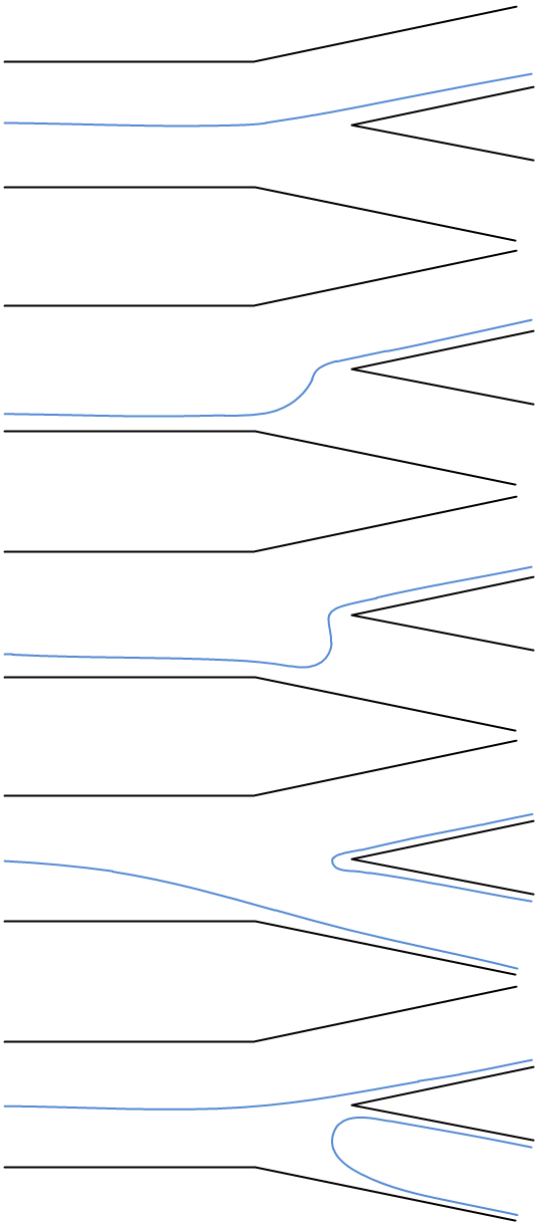

Figure 4-8 a) to e) from top to bottom. Interface breaks and a large portion of organic liquid leaves through the aqueous outlet.

The distinction between the two series mentioned in point 2 is the size of the detached organic droplet, which is larger in the series 4-8.

It must be noted that individual droplets are very hard to see, even on individual frames. The droplet in figure 4-7g) is not present in an individual frame as such, but rather as a smudge. Its size is an approximation based on the size of the droplet just before detachment. This motion blur that causes the smudge also affects the figures in the third series. Although the interface around the Y-splitter island in figure 4-8d) can be seen quite clearly, the bottom interface in figure 4-8d) cannot be seen completely in the frame and was extended for clarity.

4.2.3 Back pressure loading

Jahromi et al. [30] developed a mathematical interfacial pressure balance model for the separation of multiphase microflows at the divergence point of a Y-shaped junction. The model is explained in the Theory section of this thesis. They found that increasing back pressure by varying the height of the outlet tubing led to complete separation in the microchannel. The same approach was tried on our systems. The advancing and receding contact angles were adopted from the paper (59° and 13° respectively) since own data was lacking at the time. All other parameters were calculated for our *IMT* chip. Based on the model, the organic outlet tubing should be elevated 39 to 52 cm with respect to the chip for complete separation. Varying the values of the advancing and receding contact angles in the model between 0° and 180° gave an organic outlet height between -6 and +53 cm.

However, in our case, application of back pressure by manipulating the outlet heights did not have an effect at all on the behaviour of the interface at the Y-splitter. The heights of both the aqueous and organic outlet tubing were varied up to 1 meter above or below the microchannel, but no effect could be observed. It is unclear why the model is not valid for our system. We also tried to vary the length of the outlet tubing to achieve complete separation, but this had no effect either.

Since a portion of the aqueous phase leaves through the organic outlet, the flow rate through the organic outlet is bigger than the organic feed. Also, the flow rate through the aqueous outlet is smaller than the aqueous feed rate since a portion of it leaks through the other outlet. With complete separation, the flow rates of the aqueous and organic phase should be equal to the aqueous and organic feed rates, respectively. We tried to fixate the flow rates of both effluents to their feed values by having two additional syringe pumps withdraw liquid from the microchannel at the same rate as it was fed. This approach failed as well, and several factors can be pointed out. The speed of the pushing and withdrawing syringe pumps was not exactly equal. In addition, making a connection between the syringes and connectors causes a small overpressure in the line, and often small air bubbles were present in the connectors or syringes which are problematic for suction.

With the *Micronit* chip, that had slightly bigger channels, the application of back pressure by varying the outlet heights did have an effect. Realtime manual manipulation of the outlet height over ±20 cm could prevent detachment of an aqueous droplet in the coated microchannel, which is described later in this thesis in section 4.3.

4.2.4 Organic leakage

In contrast to the aqueous leakage observed with all pure solvents tested, with some extractant solutions (extracting agent dissolved in an organic solvent) the opposite organic leakage was observed at the Y-splitter. This was the case for the extractant solutions E01 (30%TBP, 16%TOA in cyclohexane), E03 (0.2M Aliquat 336 in 1,3-diisopropylbenzene) and E04 (0.2M Aliquat 336 in 2-nonanone). As can be seen in figure 4-9, the interface starts at the aqueous side of the Y-junction (organic infiltration) and runs of through the aqueous outlet channel (organic leakage). The same type of leakage was reported for the MEK/water system [11].

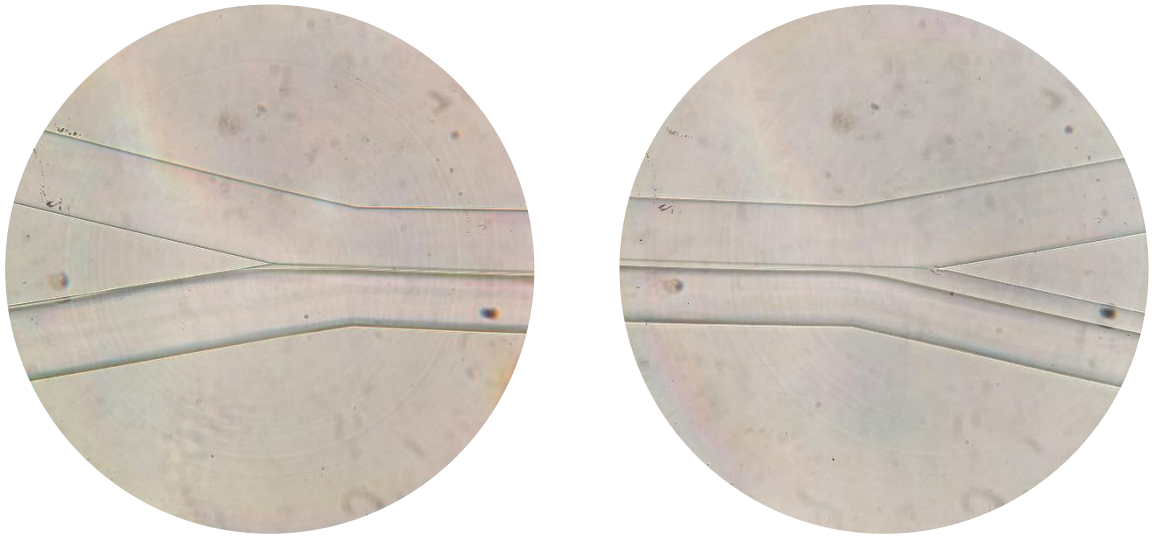

Figure 4-9. a) Organic infiltration at the inlet (left) and b) organic leakage at the outlet (right).

Instead of aqueous leakage where we believe the wall to be wetted preferably by the aqueous phase, we observe organic leakage and we believe the wall is preferably wetted by the organic phase (E01, E03 and E04). A similarity between these three extractant solutions that showed organic

leakage is the presence of a very viscous extractant. Both trioctylamine and Aliquat 336 (a quaternary ammonium salt with octyl and decyl chains) have high viscosities, 15 mPa.s [52] and 1500 mPa.s [53] respectively. To help understand what factors play a role in the reversion of the interface behaviour, immersed contact angle measurements were conducted. The results can be found in table 4-3 and the corresponding pictures in figure 4-10.

	Receding	*Static*	*Advancing*
air	-	21 ± 1.1	-
cyclohexane	-	43 ± 3.0	62 ± 1.7
E01	51 ± 0.1	101 ± 9.9	108 ± 3.3
E03	131 ± 4.9	169 ± 2.1	161 ±2.6

Table 4-3. Static and dynamic contact angles of water on an untreated glass surface in different media. Dashes indicate that a measurement could not be made. The numbers behind the ± sign are the standard deviations.

Figure 4-10. Pictures of droplets of water on an untreated glass surface in – from left to right – cyclohexane, E01 (TBP and TOA in cyclohexane) and E03 (Aliquat 336 in 1,3-diisopropylbenzene). The white background is the organic medium and the droplets are dark/have dark edges.

When the contact angle is smaller than 90°, the surface is preferably wetted by the aqueous phase, and when the contact angle is greater than 90°, the surface is preferably wetted by the organic phase. As can be seen in table 4-3, the static contact angle of water in cyclohexane is 43°. The glass surface is thus preferably wetted by the aqueous phase, which supports our observations of aqueous leakage. With the extractant solutions E01 and E03, the static contact angle of water in these solutions is greater than 90° (101° and 169°, respectively). In these cases, the glass surface is preferably wetted by the organic liquids.

It must be noted that the measured advancing contact angle of water immersed in E03 is smaller than the measured static contact angle. This should not be possible as the static contact angle lies between the minimum receding and maximum advancing angle. Measuring the dynamic angles is much harder than measuring the static one since a growing or shrinking droplet can move out of focus of the camera. Also, the baseline against which the software calculates the angle has a huge influence on the determined value, and with blurry images, the baseline sometimes needs to be adjusted for the software to make a calculation. In general, the static values have a higher accuracy than the dynamic values. The fact that the advancing angle is bigger than the static angle is considered an experimental error.

Based on these observations, it is not excluded that viscosity might play a role, but it is confirmed that surface and interfacial energies play a major role in the reversion of the interface behaviour.

Figure 4-11 shows a picture of an immersed contact angle measurement. Three aqueous drops can be seen lying on a glass slide inside the macro-cuvette that is partially filled with organic liquid. The pipette tip that dispenses the liquid is in the centre of the picture. The blue light is for contrast.

Figure 4-11. Immersed contact angle measurement in the macro-cuvette.

4.3 Surface modification

As described in the previous chapters, leakage of one phase into the outlet channel of the other phase can occur due to both outlet channels having the same surface characteristics. To overcome this problem, we applied a hydrophobic coating to the glass. The coating agent selected was octadecyltrichlorosilane (OTS), as described in the Theory section.

A cheaper glass chip (obtained from *Micronit*) was used as a substrate instead of the much more expensive *IMT* glass chip, which was used for all other experiments.

In contrast to the *IMT* chip, a laminar two-phase flow (water and cyclohexane) could not be obtained in the uncoated microchannel of the *Micronit* chip. The two microfluidic chips differ in dimensions (see Appendix 9.5 and/or section 3.2) and manufacturing method. Especially the latter is thought to influence the behaviour of the chip. The microchannel on the *IMT* chip is etched chemically which results in a very smooth surface [32]. The microchannel on the *Micronit* chip is powder blasted which results in a much rougher surface [33], clearly visible through the microscope. Although the behaviour of the two chips was not the same, coating of the *Micronit* chip was done anyway to test for the possibility of changing the surface characteristics of one outlet selectively.

After applying the coating to one of the outlet channels, syringes with water (possibly coloured with methylene blue) and cyclohexane, respectively, were connected to the two inlet channels of the *Micronit* chip to test the chip's behaviour. A few lessons were learned:

1. The OTS coating could be easily applied. Literature offered numerous (different) methods, often with difficult cleaning pre-steps [24], and focussed on precise water content and even temperature [25]. In practice, a hydrophobic surface was obtained within a few minutes without precise control of the water content and without taking temperature into account. The coating might not have been present as a perfect monolayer, but for our purpose this was not relevant.
2. The sections of the glass microchannel coated by the OTS were fully wetted by the organic phase. The aqueous phase, present as droplets in the organic medium, did not touch the now coated wall.
3. The pump rate and thus fluid velocity inside the microchannel is of importance during the coating process as the OTS spreads radially in the microchannel, either via diffusion or convection. The radial spreading of the OTS results in the unwanted coating of the opposite wall after a certain distance in the channel.

Pictures of the coated *Micronit* chip can be seen in figure 4-12. The left picture shows the middle section of the microchannel, of which the left $1/5^{th}$ is coated on both sides and the right $4/5^{th}$ is only coated on top. The right picture shows the end of the microchannel. The top wall and outlet branch are coated with OTS (hydrophobic channel walls) while the opposite wall and outlet branch remain untouched and hydrophilic. For a water-cyclohexane system at flow rates of 40 µl/min, a two-phase laminar flow can be obtained in the *Micronit* microchannel as can be seen in figures 4-12a and b. The droplet flow in the completely coated (left-most) section of the microchannel changes into parallel flow when the droplet hits the uncoated hydrophilic (bottom) wall. Furthermore, it is clear from figure 4-12b that there is no aqueous leakage where the aqueous phase is in contact with the wall of the organic outlet channel (such as depicted in figure 4-2b).

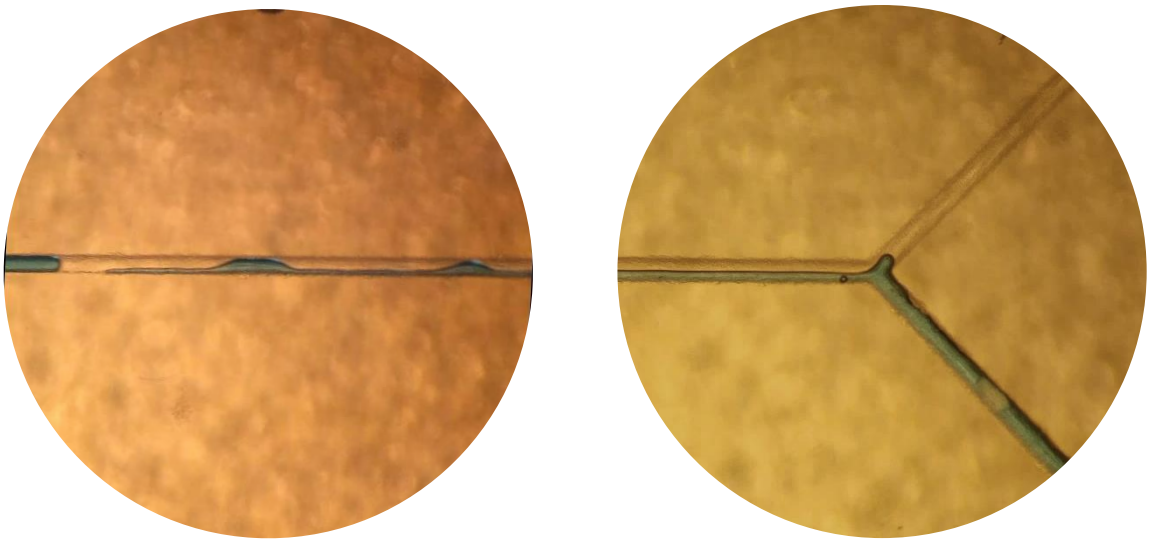

Figure 4-12. Two microscopic views of the partially coated Micronit microchannel. a) Middle section of the microchannel. b) Right section of the microchannel plus Y-splitter. Organic phase is cyclohexane (transparent) and the aqueous phase is dyed with methylene blue (blue).

Some leakage remains, however, and droplets of water detach from the interface at the Y-splitter and leave through the organic outlet (surrounded by organic liquid). In figure 4-12b, a blue aqueous droplet can be seen at the Y-splitter that is one the verge of detaching from the interface. As mentioned in section 4.2.3, this kind of leakage (droplet detachment) could be stopped by real-time application of a back pressure while looking at the Y-splitter. Since remaining leakage (droplet detachment) does not touch the wall and can be either induced or stopped by application of a (negative) backpressure, the leakage is thought to be due to pressure differences resulting from different hydraulic resistances in the outlet channels and tubes. Most importantly, however, the experiment shows that the aqueous leakage due to surface effects in our system can successfully be stopped by application of a coating, as in previous reported work [50].

4.3.1 Removal of the hydrophobic coating

After the successful application of the coating, we tried to remove the coating again from the *Micronit* chip. The ability to remove the coating was a requirement before applying it to the *IMT* chip, of which we had only one and was quite expensive. It could either be necessary to restore the microchannel to its original state for other experiments, or mistakes in the application of the coating could be made (coating unwanted parts of the microchannel). UV light was used as it is a common technique to create patterning on substrates [54].

Short wave (254 nm) UV light had no apparent effect, even after several days of non-stop exposure. The reason is that the Pyrex glass blocks short-wave UV light up to roughly 270 nm [55]. Long-wave (365 nm) UV light did have an effect, and after 48 hours of exposure, the coated microchannel was no longer completely wetted by the organic phase. Instead, the behaviour of the fluids resembled the behaviour on the untreated control chip, but a remarkable difference remained.

In the coated and UV exposed microchannel, bubbles were seen to grow at the walls of the microchannel, as can be seen in figure 4-13. This is probably desorption of air, that was previously dissolved in the water, to the wall. As mentioned before, an intact coating is completely wetted by the organic phase, effectively preventing the aqueous phase from touching the wall. When the coating degrades, it is thought that the decreased hydrophobicity no longer prevents the aqueous phase from touching the wall. The hydrophobic sites left now act as nucleation sites for the dissolved air to degas and form bubbles in the microchannel. Flowing degassed water through the microchannel produced no bubbles, supporting this explanation.

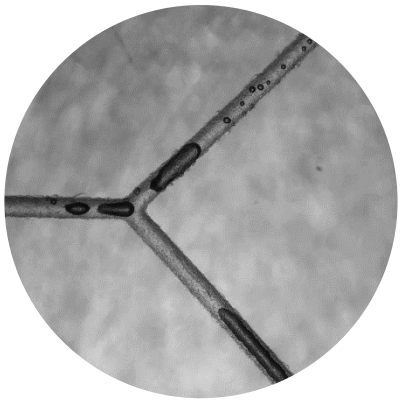

Figure 4-13. Formation of gaseous bubbles (dark) in the microchannel (Micronit chip).

Hydrophobic surfaces are used in microfluidics in so-called degassing plates to capture bubbles [56], but this phenomenon has, to our knowledge, not been described associated with a degradation of coating in two-phase flow.

To quantify the degree of coating or hydrophobicity, contact angles were measured again. Since the contact angle cannot be measured inside the microchannel, glass microscope slides were subjected to a similar coating (and removal) procedure and subsequently contact angles were measured. The measured contact angles can be found in table 4-4 below. All angles are an average of at least three measurements. As can be seen in table 4-4, the UV treatment had very little effect on the contact angle, it decreased only from 109° to 105°. This seems contradictive with the described observations, where the behaviour resembled that of the untreated chip. Perhaps this small decrease in contact angle is just enough to no longer have complete wetting by cyclohexane.

Blank glass	21 ± 1.1
OTS coated glass (control)	109 ± 0.2
OTS coated glass + UV light	105 ± 1.5
OTS coated glass + KOH/MeOH	39 ± 6.0

Table 4-4. Static contact angles of water on various (un)treated glass surfaces in air. The numbers behind the ± sign are the standard deviations.

To completely remove the hydrophobic coating of glass sample slides, a 1 M solution of potassium hydroxide in methanol was suggested by another group at the TU Delft and tried. After one week of immersion in the solution, the contact angle was still significantly larger than untreated glass (determined by sight, not measured). After 4 weeks of immersion, the contact angle was measured and found to be 39° as given in table 4-4. Although the contact angle has decreased a lot, this method is not feasible for usage on the *IMT* microfluidic chip. It requires soaking the chip in a strongly alkaline solution for over a week, potentially damaging the fine guide structure in the microchannel. Treatment with piranha solution (a solution of concentrated sulfuric acid and 30% hydrogen peroxide) was not possible because of plastic parts of the chip (and its connections) and oxygen-plasma cleaning was not available in our lab.

Since no method was found to safely and completely remove the hydrophobic coating, it was decided to not apply the OTS coating on the more expensive *IMT* chip. Partial removal by UV light would result in bubble growth in the microchannel which disrupts laminar flow and complete removal by KOH/MeOH could potentially damage the chip.

4.3.2 Radiation effects on the hydrophobic coating

Although the coating was not applied to the IMT chip and used for liquid-liquid experiments, it was investigated how the coating would degrade under influence of radiation. Glass substrates were coated with the silanizing agent, subjected to various doses of gamma radiation (1 to 40 kGy) and subsequently the contact angle of water on these substrates was measured. During these experiments, a clear discolouration of the glass substrates could be seen from transparent to yellowish or brownish. A picture of the discolouration of the glass slides is included in figure 4-15.

The expected decrease in contact angle upon increased absorbed dose is visible in figure 4-14. The contact angle on a fresh, non-irradiated substrate is about 104°. Irradiation up to 5 kGy does relatively little harm and the contact angle decreases only to about 100°. Irradiation up to 10 kGy shows a sharp decrease in the contact angle, after which it is not affected much more. The spread between the different measurements is quite large, especially at 20 kGy, but the average values remain between 70° and 80°.

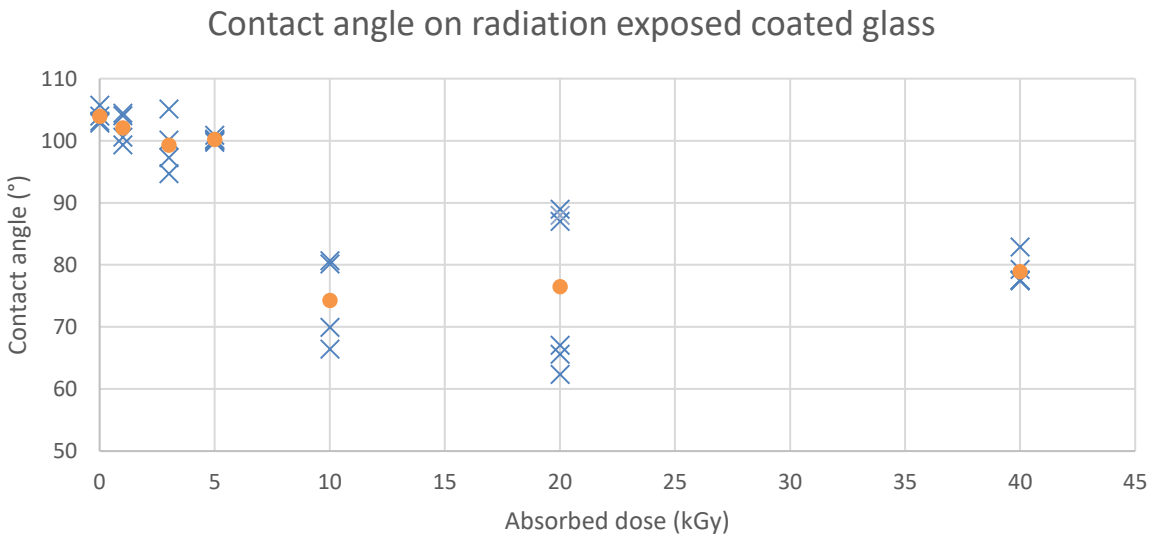

Figure 4-14. Contact angle of water on irradiated, hydrophobically-coated glass as a function of absorbed dose. The absorbed dose comes from gamma quants emitted by a Co-60 source. Blue crosses are individual measurements, orange circles represent the average values.

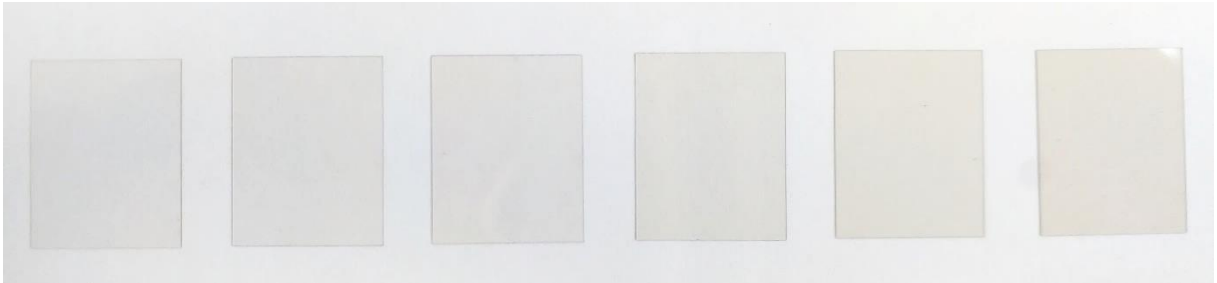

Figure 4-15. Discolouration of the irradiated coated glass substrates. From left to right: 1, 3, 5, 10, 20 and 40 kGy.

In conclusion, the threshold value for degradation of the OTS coating is 5 kGy. The radiation causes breakage of chemical bonds in the hydrocarbon tail of the coating. When a C-C bond is broken, the hydrocarbon tail becomes shorter and therefore less hydrophobic. When the Si-C bond is ruptured the hydrocarbon tail detaches completely, leading to less surface coverage which also decreases the hydrophobicity. Whether the degraded coating with a contact angle of roughly 80° is still usable depends on the application and was not investigated.

4.4 Radioactive extraction

Several liquid-liquid extraction experiments were done to determine the best solvent combination for the separation of rhenium from tungsten. As organic phase, seven extractant solutions (E01-E07) and four pure organic liquids (2-pentanone, 2-nonanone, tributyl phosphate and MEK) were tested. The aqueous phase consisted of 0.1 mg/ml NH_4ReO_4, 1 mg/ml Na_2WO_4 and 0.01M HCl and contained either Re-186/188 or W-188. The aqueous phase was chosen based on previous work of Ilza Dalmázio, who found that this composition yielded the highest efficiencies in extractions with MEK [11]. Choosing the same aqueous phase would make a comparison with these previous results possible. What must be noted is that the aqueous phase was found to be unstable, i.e. over a week after preparation, a yellowish precipitate could be observed. This was not previously observed. Solutions therefore were made fresh every week and the instability is not thought to have influenced the results presented in this thesis. Furthermore, the extraction efficiencies given are relative, i.e. the count rate found in an aliquot of either phase is not related to the count rate of the aqueous phase added, but to the sum of the count rates measured in both phases after extraction. Equation 2-10, as stated in the Theory section, is given again:

$$Relative\ extraction\ efficiency = \frac{R_{org}^{after}}{R_{aq}^{after} + R_{org}^{after}} \cdot 100\% \qquad 2\text{-}10$$

4.4.1 Conventional batch extraction

Liquid-liquid extraction experiments were first done as a conventional batch experiment. The extraction efficiency of rhenium for different extracting phases is given in figure 4-16 as dark blue bars. Experiments were done (at least) in triplet and the error bars indicate the standard deviations.

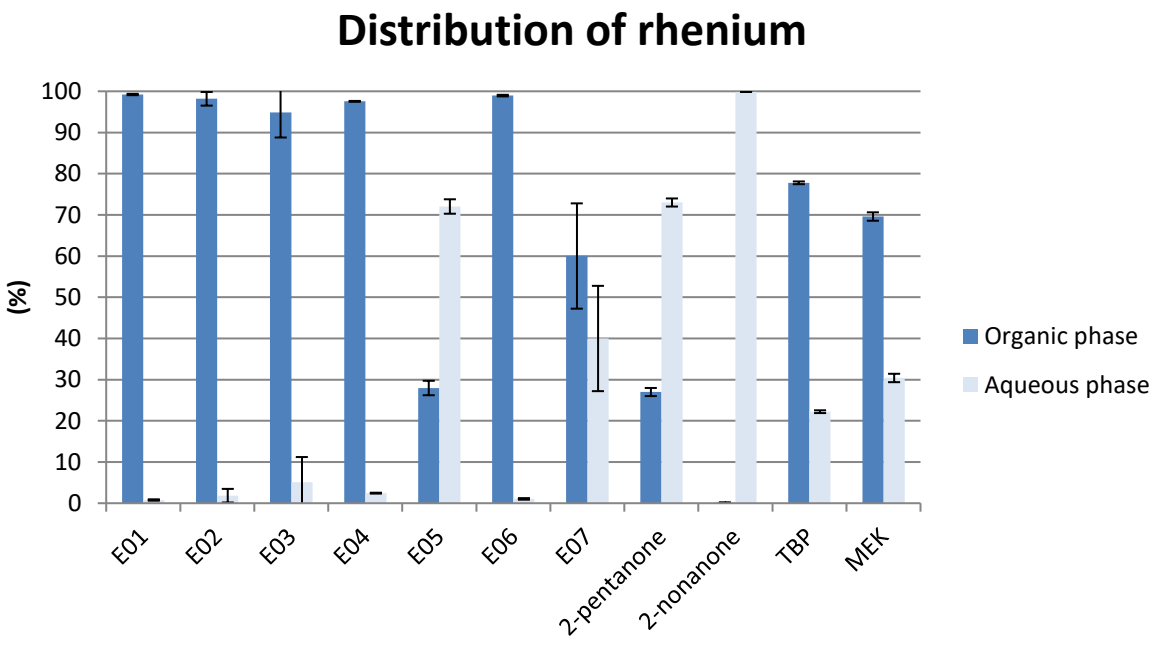

Figure 4-16. Distribution of rhenium in different extracting liquids. The values of the organic phase (dark blue) bars equal the relative extraction efficiency of rhenium. Error bars indicate standard deviations.

As can be seen in figure 4-16, five extractant solutions (E01, E02, E03, E04 and E06) perform well and all have extraction efficiencies >90%.

E05 (0.1M TOPO in cyclohexane) and E07 (0.1M TIOA in cyclohexane) have low efficiencies. For extractant solution E05, an extraction coefficient for Tc(VII) from an acidic aqueous solution (1N H_2SO_4) is reported to be 41 [29]. However, for the extraction of technetium from a neutral aqueous solution (1N Na_2SO_4) the extraction coefficient is reported to be 0.051. The fact that our aqueous phase (0.01M HCl) is less acidic is a probable reason for the low extraction efficiency. For E07, the same reasoning applies. The reported extraction coefficients are 72 and 0.003 for aqueous phases of 1N H_2SO_4 and 1N Na_2SO_4, respectively [29].

With the problem of the aqueous leakage on the microchip in mind, extractions were also done with the aqueous phase additionally coloured with methylene blue. The reasoning was that the blue colouring would make it easier to detect the aqueous phase contaminating the organic effluent, after which its collection could be manipulated manually (i.e. putting the effluent to waste when blue droplets are visible in the outlet tubing or pipetting pure organic phase out of the collection vial after collection). However, it was found that upon addition of methylene blue to the aqueous solution, the dye formed flakes and precipitated. The presence of tungsten (and possibly rhenium) in the aqueous solution probably led to the precipitation and it is highly likely that the tungsten precipitated together with the dye. Because of this, the results of this experiment were discarded. Later tests showed that another dye, Water Blue, did not cause precipitation but no extractions were done with this dye due to time limitations. To the best of our knowledge, the precipitation of methylene blue in the presence of tungstate has not been described in literature.

In a second experiment, the distribution of tungsten was determined, and the results are given in figure 4-17. Experiments are again done (at least) in triplet and the error bars indicate the standard deviations.

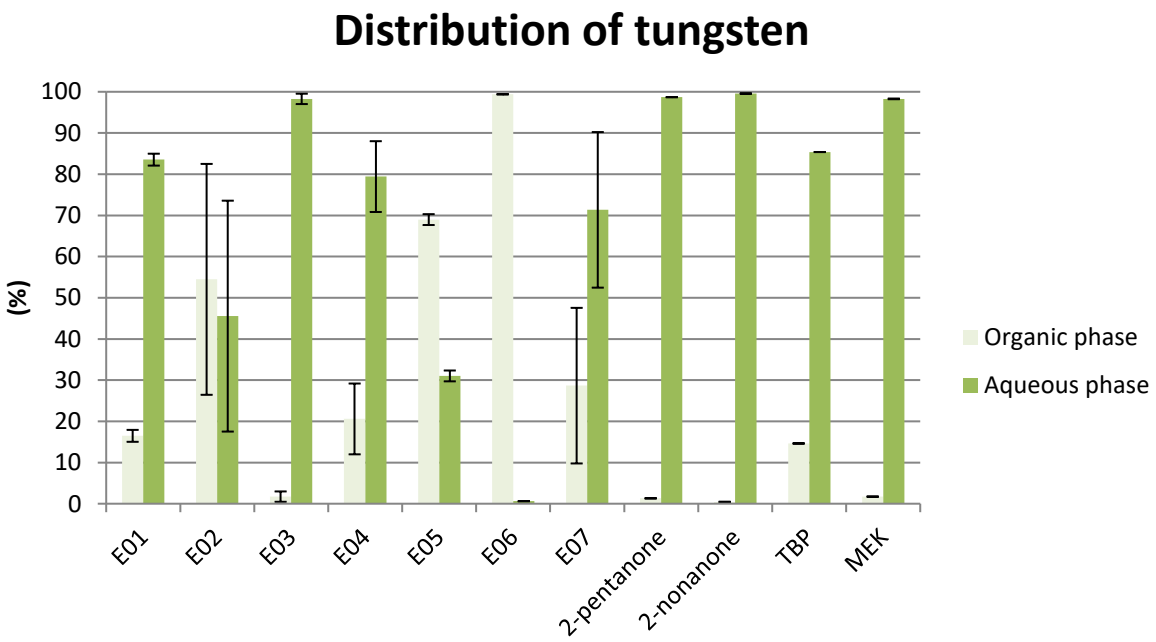

Figure 4-17. Distribution of tungsten in different extracting liquids. The values of the organic phase (light green) bars equal the relative extraction efficiency of tungsten. Error bars indicate standard deviations.

Only E03, MEK (2-butanone), 2-pentanone and 2-nonanone have low (desired) extraction efficiencies for tungsten.

2-Butanone, 2-pentanone and 2-nonanone are chemically very similar. They have the same functional ketone group and differ only in the length of their hydrocarbon chain. They show similar

behaviour and their efficiency towards tungsten is very low. However, it is well-known [57] that a longer hydrocarbon tail negatively influences the extraction efficiency of rhenium. The results in figure 4-16 confirm this, extraction efficiencies of less than 30% for 2-pentanone and practically 0% for 2-nonanone render these two solvents useless for our application.

For E03 (0.2M Aliquat 336 in 1,3-diisopropylbenzene) the desired combination of a high efficiency for rhenium and a low efficiency for tungsten is observed. The measured efficiency for tungsten is equal to that of MEK (both 1.3%), while the measured efficiency of rhenium is even better (95% vs 70%). However, both the extractant as the solvent in E03 have high boiling points and thus E03 cannot be evaporated as easily as is done with MEK based systems [2]. An additional back-extraction step would most probably be necessary. However, this is considered out of scope for this thesis and was therefore not looked in to.

4.4.2 Microfluidic extraction

Microfluidic extractions on the *IMT* microchip were done with the extractant solutions E01, E03 and E04, as these showed favourable wetting of the microchannel. With the equilibrium values of the extraction efficiency known from the experiments described in the previous section, it was investigated how the extraction proceeded in the microchannel.

Flow rates were chosen so that the interface did not leak through the organic outlet (no aqueous leakage), while at the same time keeping the amount of organic phase that leaves through the aqueous outlet (organic leakage) as low as possible.

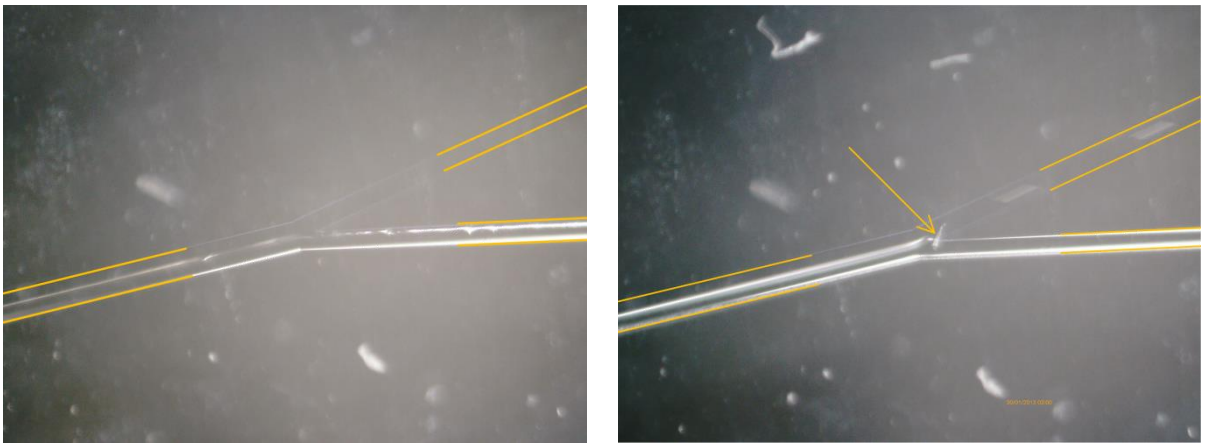

Figure 4-18. Microscopic pictures of the Y-splitter during active extraction, aqueous phase shows white lining, organic phase is barely visible. The contours of the beginning and ends of the channel are indicated with orange. a) no aqueous leakage (left), b) droplets of aqueous phase leave through organic outlet through a fibre (indicated with orange arrow) stuck at the splitter (right).

In figures 4-18 pictures are shown of the experiments as observed through the digital microscope used for radioactive experiments with Re-186/188 in the microchannel. As can be seen, it is quite difficult to distinguish the walls and especially the interface. The aqueous phase in the bottom half shows a white lining while the organic phase is completely transparent. This makes it possible to have some distinction. It was continuously monitored that there was no aqueous leakage so that a pure organic phase could be collected. Various disturbances in pumping rate called for minor adjustments to keep the interface at the desired position. Incidentally an experiment had to be stopped when for instance a small fibre stuck at the splitter (see figure 4-18 b).

The extractions were run at different flow rates to get aqueous contact times of approximately 0.6, 1.1 and 2.3 seconds (40, 20 and 10 µl/min of aqueous phase, respectively). The results are presented

in figure 4-19. A few things must be noted beforehand. The flow rates of the aqueous and organic phase are not equal but set so that the interface is at the desired position, and this ratio differs per organic phase. The ratios are given in table 4-5. The ratios were determined experimentally – by trial and error – without an initial guess with Pohar's relationship [22] since viscosities of the solutions were unknown.

Extractant solution	Ratio (aqueous : organic)
E01	1.39 : 1
E02	1.59 : 1
E03	1.38 : 1

Table 4-5. Extractant solutions and their aqueous : organic flow rate ratio.

The extraction efficiencies presented are corrected for the differences in aqueous and organic flow rate by dividing through the ratio, as explained in equation 2-9 in the Theory section. This way, the maximum activity possible would be 100%. The equation is given below:

$$Extraction\ efficiency = \frac{1}{ratio}\frac{[R]_{org}^{effluent}}{[R]_{aq}^{feed}} \cdot 100\% \qquad 2\text{-}9$$

$$= \frac{R_{org}^{effluent}}{R_{aq}^{feed}}\frac{V_{aq}}{V_{org}}\frac{100\%}{ratio} = \frac{R_{org}^{effluent}}{R_{aq}^{feed}} \cdot 100\%$$

Not correcting for this ratio would yield extraction efficiencies greater than 100% since the count rate per milliliter of organic effluent can (and was measured to) be greater than the count rate per milliliter of aqueous feed. This would be misleading since less volume of organic phase was collected in total. The activity is, however, concentrated in the organic phase due to the differences in flow rates.

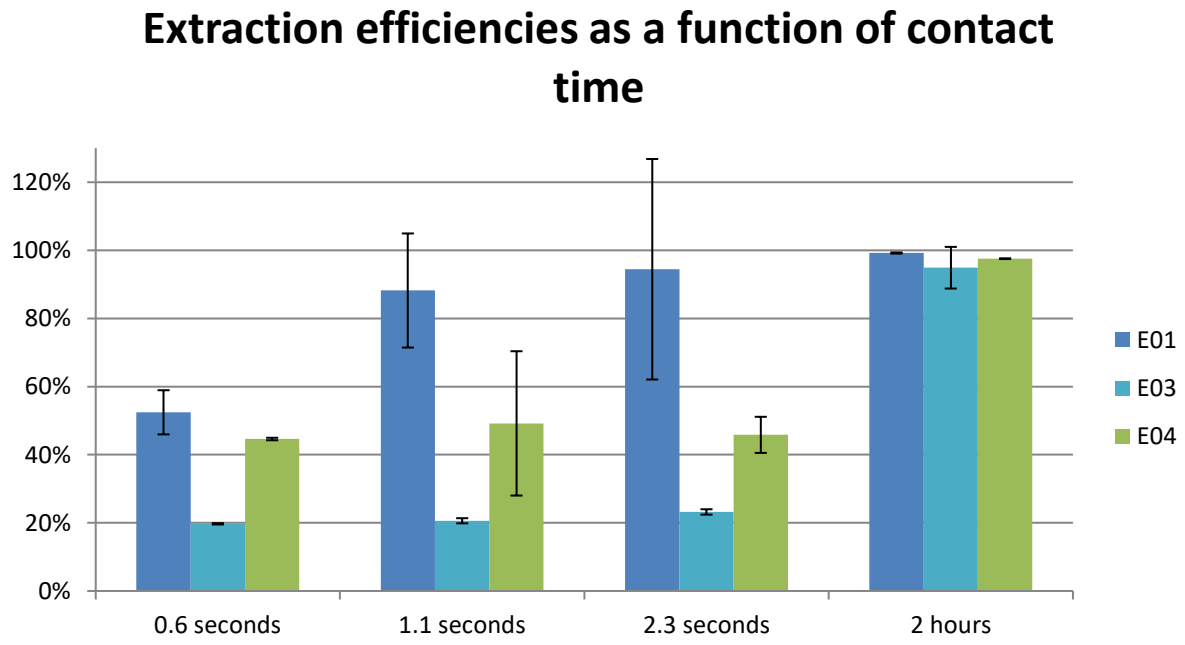

Figure 4-19. Extraction efficiencies of extractant E01 (30%TBP, 16%TOA in cyclohexane), E03 (0.2M Aliquat 336 in 1,3-diisopropylbenzene) and E04 (0.2M Aliquat 336 in 2-nonanone) as a function of aqueous contact time. The extractions with 0.6, 1.1 and 2.3 seconds contact time were done in the microchannel, the extraction with hours-contact time was done in conventional batch. Aqueous to organic flow rate ratios are 1.39, 1.59 and 1.38 for E01, E03 and E04 respectively. Error bars represent standard deviation.

As can be seen from figure 4-19, E01 performs very well on the *IMT* microchip with an extraction efficiency for rhenium reaching 94%. Two things catch the eye, the variation between the different collected fractions is large and one of the ratio-corrected data points even exceeds 100%. An explanation could be the laminar flow in the channel. Slower flowing regions near the walls have longer residence times, potentially achieving more activity per volume. When the laminar flow is disrupted by for instance an air bubble shooting through the channel, all saved up activity in the channel is eluted at once.

E03 and E04 perform less well, with maximum efficiencies achieved in the microchannel of 23% and 46%, respectively. The mass transfer is slower, presumably because of the higher viscosities of the extractant solutions. Although the equilibrium values after two hours for E03 are very favourable, longer contact times, and thus longer microchannels, are needed for high efficiencies in the microchannel.

4.5 Membrane separator

Because of the difficulties with phase separation on a Y-Y channel microfluidic chip, a different separation method was explored, and a membrane separator was purchased from Zaiput Flow Technologies.

The membrane separator was tested with mixtures of (methylene blue dyed) water and several (immiscible) organic liquids (n-dodecane, cyclohexane, 1,3-DIPB, 2-nonanone and dichloromethane). It worked instantaneous for all tested liquids and complete separation was obtained. It truly is a plug and play device that does not need worrying when in operation.

The main disadvantage of the membrane separator, especially for research purposes, is that it is difficult to clean. A simple rinse does not clean the device sufficiently, mostly because of 'dead zones' at both sides of the diaphragm. Also, a dry device is favoured over one that has (rinsing) fluid left inside as it is unclear when the effluent correctly represents the experiment due to mixing inside the device. However, drying of the device with pressurized air is difficult from a radiation safety perspective because of the formation of aerosols, as well as due to high boiling components in some organic phases (>200 °C) that are not easily evaporated. The device can be opened and wiped dry – except for the wetted side of the diaphragm – but opening would also result in contamination of the entire device with activity.

Because of the above-mentioned disadvantages, it was decided to run extractions without activity and analyse the aqueous effluent by ICP-OES.

4.5.1 MEK/water system

Although the organic phase in the MEK/water system can be separated in the microchip without contamination with aqueous phase, a portion of the organic phase leaves through the aqueous outlet resulting in efficiency losses. Complete separation in the membrane separator could potentially increase the overall efficiency and thus the membrane separator was tested for the MEK/water system.

As can be seen in figure 4-20, complete breakthrough of the blue aqueous phase through the membrane happened. All liquid – organic and aqueous – left the membrane separator through the organic outlet. The experiment was repeated with a new membrane to exclude a broken membrane and without the methylene blue dye to exclude any interference, but the complete breakthrough of aqueous phase remained.

Figure 4-20. Breakthrough of aqueous phase. Light blue is the organic phase, dark blue is the aqueous phase coloured with methylene blue dye. Front tubing is the organic side of the separator, back tubing is the aqueous side of the separator.

The membrane separator was tested with solely an aqueous feed that was slightly undersaturated with MEK (5 ml MEK-saturated water + 100 µl water). The under saturation was chosen as a safety margin so there would not be (traces of) an organic phase. Again, all effluent left through the organic outlet. It was concluded that the MEK dissolved in water alters the surface tension of the aqueous phase such, that it also wets the hydrophobic membrane. Because of the miscibility of both phases, the membrane separator cannot be used for the MEK/water system.

4.5.2 Membrane separator behind IMT chip

To evaluate the liquid-liquid extraction behaviour of the organic phases that showed aqueous leakage on the microchip, the membrane separator was placed behind the *IMT* chip to ensure complete separation and the recovery of two pure phases. One of the outlets of the *IMT* chip was closed off and a connector was modified so it could connect the two different sizes of tubing. The experiment was run with the immiscible extractant solutions that showed highest efficiency for rhenium extraction, i.e. E01, E02, E03, E04 and E06. The experiment was also conducted with an aqueous phase containing lutetium and a corresponding organic phase of 10% DEHPA in dihexyl ether [16]. The aqueous effluent was analysed with ICP-OES and the results are given in table 4-6.

Extractant solution	*Extraction efficiency rhenium (%)*
E01	99.7 ± 0.03
E02	99.5 ± 0.05
E03	93.6 ± 0.14
E04	96.9 ± 0.21
E06	18.6 ± 0.42
	Extraction efficiency lutetium (%)
10% DEHPA in dihexyl ether	99.5 ± 0.01

Table 4-6. Extraction efficiencies for rhenium and lutetium with different extractant solutions. 20 µl/min aqueous flow rate. Membrane separator installed behind IMT chip. Value after ± sign is one standard deviation.

What stands out are the high efficiencies compared to the values found without the membrane separator (with solely the *IMT* chip). The contact time between the two phases increases drastically with the membrane separator connected. The aqueous contact time inside the microchannel remains 1.1 seconds, but the mixture takes about 45 seconds to reach the separator and another 11 minutes to pass through the membrane section of the separator at the chosen flow rate (20 µl/min aqueous flow rate). 18 minutes after the start of the experiment the first aqueous phase was collected, but in the last 7 minutes both phases were already separated and passed the pressure-regulating diaphragm section of the membrane separator.

An explanation for the low efficiency of E06 in this experiment has not been found. The extraction efficiency after 2 hours found in a conventional extraction is 99%, which is far better than the 19% found in this experiment. Kinetics could be much slower, although there is no indication for this. The simple explanation is an experimental error.

The dead volume of the membrane separator is 400 µl without tubing while the dead volume of the microchannel is about 0.8 µl, which is a factor 500 smaller. It does not make sense to connect a single microchannel to the membrane separator since either only a fraction of the membrane separators capacity is used, or the residence time in the microchannel becomes so tiny that it becomes obsolete (and only creates unnecessary pressure loss). Multiple parallel microchannels could be used to increase the throughput while keeping the contact time equal, but microchannels are not necessary per se. With a membrane separator there is no longer need for difficult parallel flow and only sufficient mixing (time) is required before separation.

4.5.3 Membrane separator behind tubing

A simple Y-connector was used as a mixer to create a droplet flow inside a long section of tubing that was then connected to the membrane separator.

The experiment was designed for the lutetium system, where total handling time needs to be kept to a minimum to prevent the spontaneous dissociation of the Lu-177m(DOTA) complex (described in the Theory section 2.1.3). With the microchannel setup, processing of 2 ml of aqueous solution could take 1.7 hours while the contact time was only 1.1 seconds. A system was thought of where most of the handling time would be contact time as well. This was achieved by having a section of tubing with a volume equal to that of the liquids handled and programming the syringe pumps such that the liquids would be injected fast into the tubing after which a back and forth rocking motion would keep the fluid in motion, followed by a fast ejection from the tubing into the membrane separator.

This simple system was first tested with cyclohexane and water dyed with methylene blue. However, two problems occurred. Firstly, very fast injection leads to coalescence of the aqueous droplets in the tubing. A picture of this coalescence can be seen in figure 4-21a. Secondly, withdrawing with the pump did not make the fluid go back. It is possible that small air bubbles in the system expand which causes a significant delay instead of the fluids flowing back immediately. This could theoretically be overcome by having an additional pump push the fluid back at the end of the tubing instead of withdrawal from the beginning, but this was not tried.

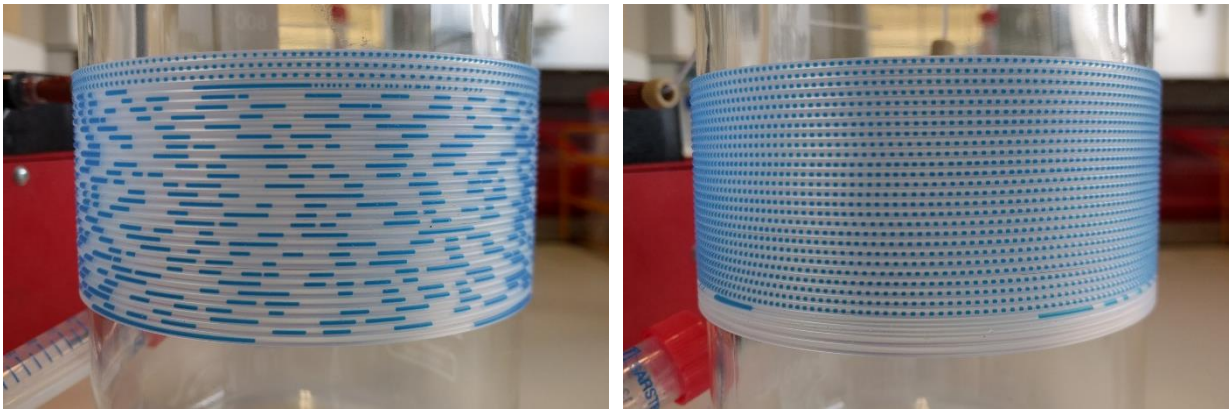

Figure 4-21. Coiled tubing, with cyclohexane and methylene blue dyed water. a) Coalescence of the droplets (left). b) Individual droplets remain intact, no coalescence (right).

The coiled tubing was kept, and instead, the liquids were pumped through at 200, 400 and 800 µl/min (corresponding to 5.33, 2.67 and 1.33 min contact time, respectively) such that there was (almost) no coalescence between the individual droplets. A picture of the system with individual,

non-coalesced droplets is given in figure 4-21b. The system was tested for rhenium with the best performing extractant solution E03 (0.2M Aliquat 336 in 1,3-diisopropylbenzene) and with 10% DEHPA in dihexyl ether against an aqueous solution of lutetium. The results for rhenium are given in table 4-7 and the results for lutetium are given in table 4-8.

Flow rate (µl/min)	*Contact time (minutes)*	*Extraction efficiency (%)*
200	5.33	95.3 ± 0.10
400	2.67	88.9 ± 0.15
800	1.33	81.5 ± 0.23

Table 4-7. Extraction efficiencies of rhenium for different contact times with extractant solution E03 (0.2M Aliquat 336 in 1,3-diisopropylbenzene). Value after ± sign is one standard deviation.

Flow rate (µl/min)	*Contact time (minutes)*	*Extraction efficiency (%)*
200	5.33	99.5 ± 0.01
400	2.67	99.4 ± 0.00
800	1.33	98.9 ± 0.04

Table 4-8. Extraction efficiencies of lutetium for different contact times with 10% DEHPA in dihexyl ether. Value after ± sign is one standard deviation.

From table 4-7, it can be seen that the extraction efficiency of rhenium is 81% after 80 seconds and reaches 95% after just over five minutes of contact time. A direct comparison with the results on the *IMT* chip is difficult, where the maximum efficiency is 22% after 2.3 seconds of contact time. However, the differences in total handling time are large. With the coiled tubing and membrane separator 2 ml of aqueous solution can be processed in 16 minutes with 95% efficiency, whereas with the microchannel the same amount of aqueous phase takes 3 hours and 20 minutes for a recovery of 23%, or 50 minutes for a recovery of 20%.

For lutetium, this is even more outspoken. With a contact time of 80 seconds, the extraction efficiency reaches already 99%. The total handling time in this case is 4 minutes. This is shorter than the current extraction step, which is about 10 minutes [16], and is promising in minimizing the spontaneous dissociation of Lu-177m from its complex.

4.6 Membrane irradiation

The PTFE membrane used in the membrane separator was irradiated with a Co-60 source to investigate the effects of radiation damage. The standard membrane with 0.5 µm pores was placed in the middle of the irradiation chamber and subjected to various doses. The results are presented in table 4-9. Membranes irradiated up to 2 kGy showed no effects on performance or failure. With the membrane irradiated up to 10 kGy, the separation was still complete, but when disassembling the separator, it was observed that the support of the membrane had become brittle and broke. With the membrane irradiated up to 40 kGy the membrane failed, and breakthrough of the aqueous phase was observed. The broken membrane support can be seen in figure 4-22.

Dose (kGy)	0.1	0.2	0.3	0.4	0.5	0.6
Membrane failure	no	no	no	no	no	no

Dose (kGy)	0.8	1	2	10	40
Membrane failure	no	no	no	no but support broke	yes

Table 4-9. Failure of the membrane (breakthrough of aqueous phase) for various irradiations in kGy.

The failure mode is therefore probably breakage of the membrane support leading to a tear in the actual membrane, resulting from pressure differences over the membrane. Apart from the support becoming brittle, which could clearly be seen by the human eye, the actual membrane was investigated for possible damage with the aid of an electron microscope. Despite charging on the highly insulating PTFE sample, reasonable pictures could be taken at magnifications up to 10.000 times.

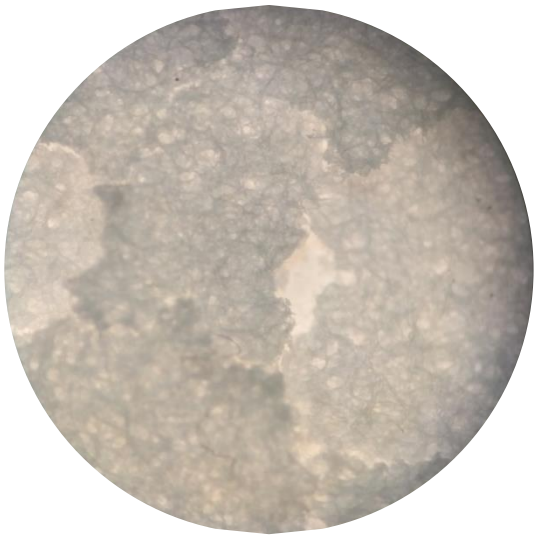

Figure 4-22. Microscope view of the broken membrane support (±16 times magnification). Actual membrane visible through a gap in the support in the centre of the image.

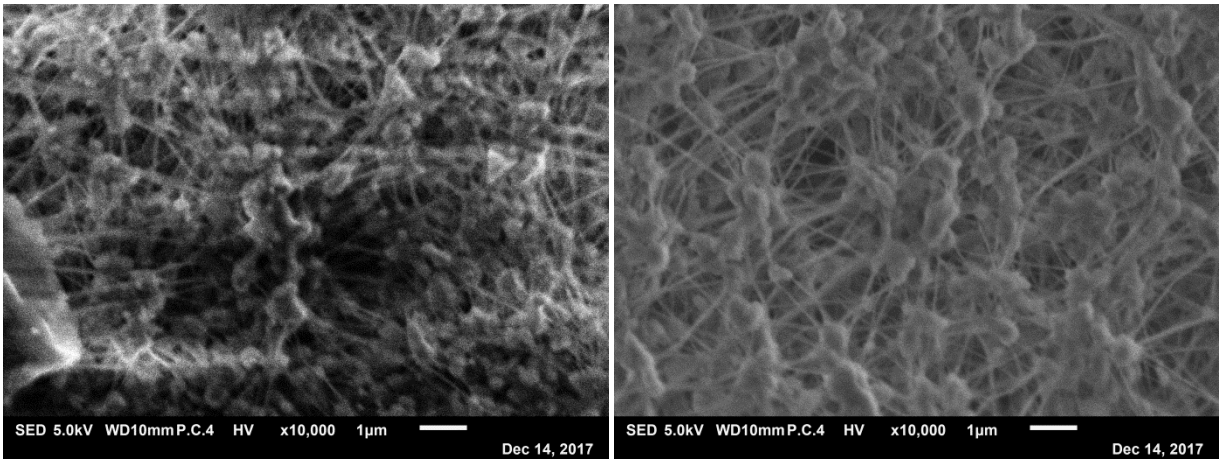

Figure 4-23. SEM pictures of the PTFE membrane at 10.000 times magnification. a) unirradiated membrane (left), b) membrane irradiated with 40kGy (right).

No signs of damage can be observed when studying the pictures in figure 4-23. The fibres that make up the membrane remain intact and no other anomalies were found. However, a tear in the membrane was not found. The optical microscope available gave insufficient magnification and with the electron microscope the search was too tedious.

Choosing a different support that is more resistant to radiation damage or adding an extra layer of a rigid fine mesh behind the membrane, might extend the lifetime of the membrane. It must be noted that the irradiation was done in air and with only gamma rays. In actual operation, the membrane would be in contact with an aqueous and organic phase, and β^--particles would be present as well. The presence of other liquids and oxygen play a role in the radicals that are formed by the ionising radiation and can affect the total damage [58]. To our knowledge, there is no literature about the effects of radiation on these kind of membranes.

5
Conclusions

This thesis addresses the separation of medical radionuclides, such as the generator pairs W-188/Re-188, Mo-99/Tc-99m, and Lu-177m/Lu-177, in microfluidic systems.

The first objective was to understand and avoid the formation of precipitate in the microchannel, which was observed in previous work in our group [11]. Since the miscible water-MEK system showed precipitation in the microchannel, a range of less miscible organic phases (pure solvents or extractant solutions) were investigated. Precipitation did not just happen with relatively miscible solvents (e.g. 2-pentanone), but also in solvents with low water solubility that contained an oxo group (e.g. tributyl phosphate and 2-nonanone). It was not possible to determine the composition of the precipitate; therefore, the formation mechanism of the precipitate could not be further investigated. No precipitation was found for solvents with low water-miscibility that did not contain an oxo group (e.g. cyclohexane, 1-3-diisopropylbenzene, and n-dodecane) and nearly all extractant solutions. It was also observed that precipitation was more likely to happen with tungsten than with molybdenum.

Conventional extractions for the W-188/Re-188 system showed that almost all extractant solutions tested have a high extraction efficiency for rhenium, but also an unwanted high extraction efficiency for tungsten. Only one extractant solution, 0.2 M Aliquat 336 in 1,3-diisopropylbenzene, was found to have a high extraction efficiency of 94.9±6.1% for rhenium and a favourable low efficiency for tungsten of 1.7±1.3%. The efficiency for tungsten was equal to the value found for the commonly used organic solvent methyl ethyl ketone (MEK), and for rhenium the efficiency was better than with MEK.

Extractions in a Y-Y microchannel were only done with a few extractant solutions, since those showed favourable behaviour in the microchannel, i.e. a pure organic phase at the outlet. The results showed large variations, possibly from disturbances in the laminar flow. For the above described well performing extractant solution, 0.2 M Aliquat 336 in 1,3-diisopropylbenzene, an extraction efficiency of 23±0.8% was reached with 2.3 seconds contact time. Mass transfer is thought to be slowed down by the high viscosity of the organic phase, so longer residence times and thus longer microchannels are needed.

The second objective of this thesis was to achieve complete phase separation when using a microfluidic system. In the Y-Y microchannel, the behaviour of all pure solvents was unfavourable for collecting a pure organic phase. The aqueous phase wetted the glass surface and leaked through the organic outlet at the Y-splitter. Varying flow rate ratios to displace the interface or playing with the height or length of the outlet tubing to balance the pressures was unsuccessful as aqueous leakage remained. To test if leakage could be avoided, a hydrophobic coating was successfully applied to a glass test-microchip and the aqueous leakage due to surface effects was shown to be halted. Removal of the coating with UV light was incomplete and removal of the coating with a KOH/MeOH solution took so long that the glass might be damaged, so the coating was not tried on the actual microfluidic chip used for the experiments. The coating was subjected to gamma radiation to see the results of radiation damage on the coating. The threshold was found to be 5 kGy after which the contact angle of water on the substrate decreased significantly, which indicates a loss of hydrophobicity.

Complete separation of the phases was achieved in a system where the liquids were brought together in tubing as aqueous droplets in an organic medium and subsequently separated with a membrane separator. For the W/Re system using 0.2 M Aliquat 336 in 1,3-diisopropylbenzene as organic phase, an extraction efficiency of 95.3±0.1% was reached after 5.3 minutes contact time. This is far longer than in the microchannel, but total handling time was reduced by a factor of 12. The tubing and membrane separator system was also used for the extraction of lutetium with 10% DEHPA in dihexyl ether as organic phase. Here, 99% extraction efficiency was reached while the total handling time was also reduced by a factor of 2 compared to the conventional procedure.

In general, the laminar flow microchannel was found very tedious to work with. Although mass transfer is very efficient due to the large surface to volume ratio, the problems associated with the system outweigh this advantage. The laminar flow is easily disturbed by pumping irregularities, air bubbles or dust fibres that get stuck in the microchannel. Most importantly, the separation at the splitter is not complete and as long as this is not the case, a microchannel is not considered a viable tool for liquid-liquid extraction. The droplet microfluidics is a much simpler and more robust system. Because of the larger channel diameter dust fibres are not a threat, precipitation is no problem because the wall sees alternately the aqueous and organic phase, and separation is complete and reliable with the membrane separator. The longer residence times because of the smaller surface to volume ratio of the droplets compared to the microchannel are compensated by a shorter total handling time.

6
Recommendations

A solution of 0.2 M Aliquat 336 in 1,3-diisopropylbenzene was found to be suitable for replacement of methyl ethyl ketone (MEK) as organic phase in the extraction of rhenium from tungsten in a microchannel. However, the two components of this solution both have high boiling points (>200 °C). Because of this, evaporation of the organic phase as is done with MEK is not very feasible and an extra back-extraction (or stripping) step may be needed. The back-extraction is considered out of scope for this thesis and remains a potential topic for further work. A topic that was not tried experimentally, but that is very interesting, is an aqueous biphasic system. Such a system would eliminate the need for hazardous and/or toxic organic compounds that might me problematic for eventual use for patients.

On the issue of phase separation at the Y-splitter, the preferred wetting of the hydrophilic glass wall by one of the phases is thought to play a major role. The presence of a guide structure is also suspected of playing a role. Further research with a guideless but otherwise identical microchannel could provide more insight. Other suggestions are to manufacture a microchannel with a guide that stops some distance before the Y-splitter. This way, the guide can stabilise the laminar flow in the channel but does not interfere with the separation at the end of the channel. Also, different types of splitters that are less sharp could be considered. The prototyping of glass chips is expensive and labour intensive while the cheaper and easier producible PDMS chips are not compatible with most solvents, so more efforts on numerical simulations are recommended.

In general, observations of the microchannel were hard with the microscope(s) on hands and capturing images through the lens even harder. A good digital microscope, possibly equipped with a high-speed camera, could improve observations and make it easier to compare them with results from models.

Coating one of the outlet ports hydrophobically with octadecyltrichlorosilane (OTS) showed that the aqueous leakage due to surface effects could be stopped. For successful use of OTS on longer microchannels there should be more control of the precise application of the coating, or removal of unwanted coating. Both are topics that require more attention.

Threshold values for radiation damage on the membrane and OTS coating were determined to be 2 kGy and 5 kGy respectively by using an external gamma source on dry samples. In actual operation, the membrane and coating would be in contact with a radioactive liquid and receive both beta and gamma radiation. Future work might include exposing the samples to both beta and gamma radiation and bringing them in contact with a liquid. This will give more accurate data as beta particles and the liquids radicals will be included.

7

Acknowledgements

I would first like to thank my supervisor professor Elisabeth Oehlke for introducing me to the interesting topic of microfluidics and radioisotopes. She has always been open for questions and discussion and helped by looking with a critical eye to this thesis. I would like to thank Pablo Serra Crespo, who is also in my thesis committee, for the time he made free for the meetings we had and the advice he gave. I have had some interesting discussions about lutetium in the microfluidic system with Rupali Bhardwaj, but unfortunately most of it is still open for future work. I would like to thank her as well and wish her success with this future work. For the good company in our room I would like to thank Folkert Geurink and Adrie Laan! I could not have finished my work without the various support, including the many irradiations, from Astrid Vermeer, Mehmet Sarilar and especially Baukje Terpstra. Special thanks to Ruben Abellon from the OM group of ChemE who let me use his glovebox for solution preparation. Henk van Doorn and Koos van Kammen from the SBD made it possible to work safely with radioactivity and occasionally provided me with some drinks in *'t Koepeltje*. Finally, I would like to thank Henk Nugteren from the PPE group of ChemE and professor Bert Wolterbeek, head of the Reactor Institute Delft, for being part of my thesis committee.

8
Bibliography

[1] K. Charlton, “The Supply of Medical Radioisotopes,” 2017.

[2] M. R. a Pillai, A. Dash, and F. F. Knapp, “Rhenium-188: availability from the (188)W/(188)Re generator and status of current applications.,” *Curr. Radiopharm.*, vol. 5, pp. 228–43, 2012.

[3] A. M. R. Pillai and F. F. R. Knapp, “Evolving Important Role of Lutetium-177 for Therapeutic Nuclear Medicine.,” *Curr. Radiopharm.*, vol. 8, no. 2, pp. 78–85, 2015.

[4] World Nuclear Association, “Radioisotopes in Medicine | Nuclear Medicine - World Nuclear Association,” 2017. [Online]. Available: http://www.world-nuclear.org/information-library/non-power-nuclear-applications/radioisotopes-research/radioisotopes-in-medicine.aspx. [Accessed: 26-Mar-2018].

[5] A. Dash, F. F. (Russ) Knapp, and M. R. A. Pillai, “99Mo/99mTc separation: An assessment of technology options,” *Nucl. Med. Biol.*, vol. 40, no. 2, pp. 167–176, Feb. 2013.

[6] D. Ciceri, J. M. Perera, and G. W. Stevens, “The use of microfluidic devices in solvent extraction,” *J. Chem. Technol. Biotechnol.*, vol. 89, no. 6, pp. 771–786, 2014.

[7] D. Mark, S. Haeberle, G. Roth, F. Von Stetten, and R. Zengerle, “Microfluidic lab-on-a-chip platforms: Requirements, characteristics and applications,” *NATO Sci. Peace Secur. Ser. A Chem. Biol.*, no. 3, pp. 305–376, 2010.

[8] M. Yamamoto, S. Taguchi, S. Sato, and N. Surugaya, “Evaluation of plutonium(IV) extraction rate between nitric acid and tri- *n* -butylphosphate solution using a glass chip microchannel,” *J. Sep. Sci.*, vol. 38, no. 10, pp. 1807–1812, May 2015.

[9] Y. Ban, Y. Kikutani, M. Tokeshi, and Y. Morita, “Extraction of Am(III) at the Interface of Organic- Aqueous Two-Layer Flow in a Microchannel Extraction of Am(III) at the Interface of Organic-Aqueous Two-Layer Flow in a Microchannel,” *J. Nucl. Sci. Technol.*, vol. 48, no. 10, pp. 1313–1318, 2011.

[10] S. Goyal, A. V Desai, R. W. Lewis, D. R. Ranganathan, H. Li, D. Zeng, D. E. Reichert, and P. J. A. Kenis, “Thiolene and SIFEL-based Microfluidic Platforms for Liquid-Liquid Extraction.,” *Sens. Actuators. B. Chem.*, vol. 190, pp. 634–644, Jan. 2014.

[11] I. Dalmázio and E. Oehlke, “Evaluation of Perrhenate Extraction with Methyl Ethyl Ketone in Microfluidic Device - Unpublished work,” 2016.

[12] K. Schwokau, *Technetium: Chemistry and Radiopharmaceutical Applications*. Wiley, 2007.

[13] R. Phaeton, Z. Jiang, E. Revskaya, D. R. Fisher, G. L. Goldberg, and E. Dadachova, “Beta emitters rhenium-188 and lutetium-177 are equally effective in radioimmunotherapy of HPV-positive experimental cervical cancer.,” *Cancer Med.*, vol. 5, no. 1, pp. 9–16, Jan. 2016.

[14] S. Banerjee, M. R. A. Pillai, and F. F. Knapp, “Lutetium-177 therapeutic radiopharmaceuticals: Linking chemistry, radiochemistry, and practical applications,” *Chem. Rev.*, vol. 115, no. 8, pp. 2934–2974, 2015.

[15] R. Bharadwaj, A. Van der Meer, S. Das, M. De Bruin, J. Gascon, H. T. Wolterbeek, A. Denkova, and P. Serra-Crespo, “Separation of nuclear isomers for cancer therapeutic radionuclides based in nuclear decay after-effects - Unpublished work,” 2017.

[16] D. Alders, “Solvent extraction to separate Lu-177 in a Lu-177m/Lu-177 generator,” Delft University of Technology.

[17] IAEA, “Decay properties for generators of short-lived radionuclides.” [Online]. Available: https://humanhealth.iaea.org/HHW/Radiopharmacy/VirRad/Eluting_the_Generator/Generator_Module/Design_principles/Non_99mTc_generators/table.html. [Accessed: 03-Apr-2018].

[18] A. Dash and F. F. (Russ) Knapp Jr, “An overview of radioisotope separation technologies for

development of ^{188}W/^{188}Re radionuclide generators providing ^{188}Re to meet future research and clinical demands," *RSC Adv.*, vol. 5, no. 49, pp. 39012–39036, 2015.
[19] S. Mandal and A. Mandal, "A simple and sensitive separation technique of 99Mo and 99mTc from their equilibrium mixture," *J. Radioanal. Nucl. Chem.*, vol. 301, no. 1, pp. 297–299, 2014.
[20] H. A. Stone, A. D. Stroock, and A. Ajdari, "Engineering Flows in Small Devices," *Annu. Rev. Fluid Mech.*, vol. 36, no. 1, pp. 381–411, 2004.
[21] E. Roy, A. Pallandre, B. Zribi, M.-C. Horny, F. D. Delapierre, A. Cattoni, J. Gamby, and A.-M. Haghiri-Gosnet, "Overview of Materials for Microfluidic Applications," *Adv. Microfluid. - New Appl. Biol. Energy, Mater. Sci.*, no. December, 2016.
[22] A. Pohar, M. Lakner, and I. Plazl, "Parallel flow of immiscible liquids in a microreactor: Modeling and experimental study," *Microfluid. Nanofluidics*, vol. 12, no. 1–4, pp. 307–316, 2012.
[23] Y. Yuan and T. R. Lee, "Contact Angle and Wetting Properties," Springer, Berlin, Heidelberg, 2013, pp. 3–34.
[24] N. R. Glass, R. Tjeung, P. Chan, L. Y. Yeo, and J. R. Friend, "Organosilane deposition for microfluidic applications," *Biomicrofluidics*, vol. 5, no. 3, pp. 1–7, 2011.
[25] a Ulman, "Formation and Structure of Self-Assembled Monolayers," *Chem. Rev.*, vol. 96, no. 4, pp. 1533–1554, 1996.
[26] Y. Masuda, K. Tomimoto, and K. Koumoto, "Two-dimensional self-assembly of spherical particles using a liquid mold and its drying process," *Langmuir*, vol. 19, no. 13, pp. 5179–5183, 2003.
[27] B. Zhao, "Surface-Directed Liquid Flow Inside Microchannels," *Science (80-.).*, vol. 291, no. 5506, pp. 1023–1026, 2001.
[28] Y. Kwon, "Partition and Distribution Coefficients," in *Handbook of Essential Pharmacokinetics, Pharmacodynamics and Drug Metabolism for Industrial Scientists*, Secondary., New York: Kluwer Academic/Plenum Publishers, 2001.
[29] G. E. Boyd and Q. V. Larson, "SOLVENT EXTRACTION OF HEPTAVALENT TECHNETIUM [1]," *J. Phys. Chem.*, vol. 64, no. 8, pp. 988–996, Aug. 1960.
[30] P. Foroozan Jahromi, J. Karimi-Sabet, Y. Amini, and H. Fadaei, "Pressure-driven liquid-liquid separation in Y-shaped microfluidic junctions," *Chem. Eng. J.*, vol. 328, pp. 1075–1086, Nov. 2017.
[31] A. Adamo, P. L. Heider, N. Weeranoppanant, and K. F. Jensen, "Membrane-Based, Liquid − Liquid Separator with Integrated Pressure Control," 2013.
[32] "IMT Custom-Made Chips." [Online]. Available: https://www.i-mt.co.jp/en/chip/custom-chip/. [Accessed: 24-Mar-2018].
[33] "Micronit 3-Pack H-Microreactor (2.7 microliter)." [Online]. Available: https://store.micronit.com/microfluidic-chips/reactor-chips/3-pack-h-microreactor-2-7-l. [Accessed: 24-Mar-2018].
[34] J. D. Catasús, Y. L. Arias, R. G. Marrero, A. A. Díaz, and I. B. Portela, "Evaluation of TBP , TOA and MEK as extractants to obtain Tc radiotracers in organic phase from 99 Mo / 99m Tc generator," pp. 26–31, 2012.
[35] R. Schurhammer and G. Wipff, "Liquid-liquid extraction of pertechnetic acid (TcVII) by tri-n-butyl phosphate: Where is the proton? A molecular dynamics investigation," *J. Phys. Chem. B*, vol. 115, no. 10, pp. 2338–2348, 2011.
[36] D. J. Pruett, "the Solvent Extraction of Heptavalent Technetium By Tributyl Phosphate," vol. 16, pp. 1157–1179, 1981.
[37] K. M. Rohal, D. M. Van Seggen, J. F. Clark, M. K. McClure, C. K. Chambliss, S. H. Strauss, and N. C. Schroeder, "Solvent Extraction of Pertechnetate and Perrhenate Ions From Nitrate-Rich Acidic and Alkaline Aqueous Solutions," *Solvent extraction and ion exchange*, vol. 14, no. 3. pp. 401–416, 2007.
[38] C. Zhan-fang, Z. Hong, and Q. Zhao-hui, "Solvent extraction of rhenium from molybdenum in alkaline solution," *Hydrometallurgy*, vol. 97, no. 3–4, pp. 153–157, 2009.

[39] "The National Institute for Occupational Safety and Health (NIOSH) - 2-Pentanone." [Online]. Available: https://www.cdc.gov/niosh/npg/npgd0488.html. [Accessed: 25-Mar-2018].
[40] S. H. Yalkowsky, H. Yan, and P. Jain, *Aqueous Solubility Data*, 2nd ed. CRC Press, 2010.
[41] "The National Institute for Occupational Safety and Health (NIOSH) - Ethylene dichloride." [Online]. Available: https://www.cdc.gov/niosh/npg/npgd0271.html. [Accessed: 25-Mar-2018].
[42] "ILO-ICSC - Chloroform." [Online]. Available: http://www.ilo.org/dyn/icsc/showcard.display?p_version=2&p_card_id=0027. [Accessed: 25-Mar-2018].
[43] "The National Institute for Occupational Safety and Health (NIOSH) - Tributyl phosphate." [Online]. Available: https://www.cdc.gov/niosh/npg/npgd0625.html. [Accessed: 25-Mar-2018].
[44] "Human Metabolome Database (HMDB) - 2-Nonanone." [Online]. Available: http://www.hmdb.ca/metabolites/HMDB0031266. [Accessed: 25-Mar-2018].
[45] "ILO-ICSC - Cyclohexane." [Online]. Available: http://www.ilo.org/dyn/icsc/showcard.display?p_version=2&p_card_id=0242. [Accessed: 25-Mar-2018].
[46] "Human Matebolome Database (HMDB) - 1,3-Diisopropylbenzene." [Online]. Available: http://www.hmdb.ca/metabolites/HMDB0013806. [Accessed: 25-Mar-2018].
[47] "Human Metabolome Database (HMDB) - Dodecane." [Online]. Available: http://www.hmdb.ca/metabolites/HMDB0031444. [Accessed: 25-Mar-2018].
[48] W. Verweij, "CHEAQS Next." 2017.
[49] C. F. J. Baes and R. E. Mesmer, *The hydrolysis of Cations*. 1976.
[50] Y. S. Huh, S. J. Jeon, E. Z. Lee, H. S. Park, and W. H. Hong, "Microfluidic extraction using two phase laminar flow for chemical and biological applications," *Korean J. Chem. Eng.*, vol. 28, no. 3, pp. 633–642, 2011.
[51] J. N. Lee, C. Park, and G. M. Whitesides, "Solvent Compatibility of Poly(dimethylsiloxane)-Based Microfluidic Devices," *Anal. Chem.*, vol. 75, no. 23, pp. 6544–6554, 2003.
[52] BASF, "Safety Data Sheet Alamine ® 300," 2017.
[53] BASF and Mining-Solutions, "Technical Information Aliquat ® 336," no. September, pp. 3–5, 2015.
[54] H. Hirama, S. Wada, J. Shimamura, Y. Komazaki, T. Inoue, and T. Torii, "Surface modification of a glass microchannel for the formation of multiple emulsion droplets," *Microfluid. Nanofluidics*, vol. 21, no. 5, p. 91, 2017.
[55] Corning, "Pyrex® Glass Code 7740 - Material Properties." [Online]. Available: http://glassfab.com/wp-content/uploads/2015/08/Corning-Pyrex.pdf. [Accessed: 26-Mar-2018].
[56] D. D. Meng, J. Kim, and C.-J. Kim, "A degassing plate with hydrophobic bubble capture and distributed venting for microfluidic devices," *J. Micromechanics Microengineering*, vol. 16, no. 2, pp. 419–424, Feb. 2006.
[57] V. I. Spitsyn, "Investigations in the field of technetium chemistry," *Chem. Rev.*, vol. 3, 1981.
[58] R. E. Florin and L. A. Wall, "Gamma Irradiation of Fluorocarbon Polymers*," *J. Res. Nationa lBureau Stand. Phys. Chem.*, vol. 65, no. 4.

9 Appendix

In Appendix 9.1, pictures are given of precipitate in the microchannel, corresponding to the findings presented in table 4-1.

In Appendix 9.2, the pictures on which the Visio drawings for the aqueous infiltration from section 4.2.1 are based, are given.

In Appendix 9.3, the video frames on which the Visio drawings for the simultaneous leakage from section 4.2.2 are based, are given.

In Appendix 9.4, the activity calculations from the VIPS system are attached, as referred to in the Methods and Materials section.

In Appendix 9.5, more information about the dimensions of the *IMT* chip are given.

9.1 Pictures precipitation

2-pentanone – 0.5% W

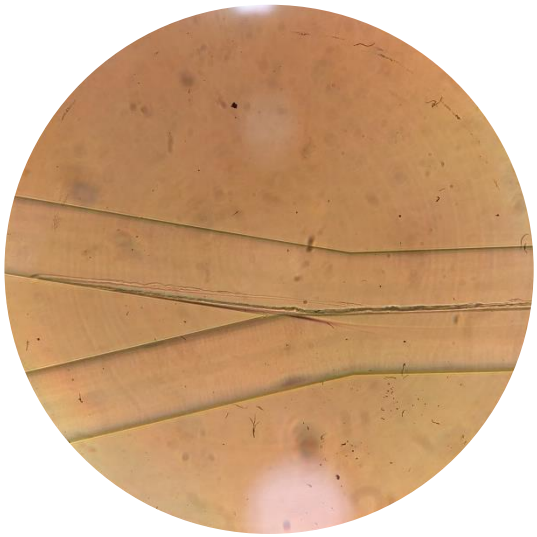

2-pentanone – 0.1% Mo

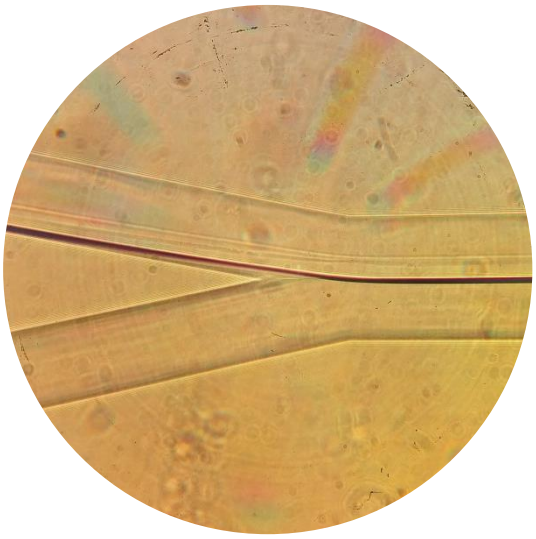

dichloromethane – 1% W

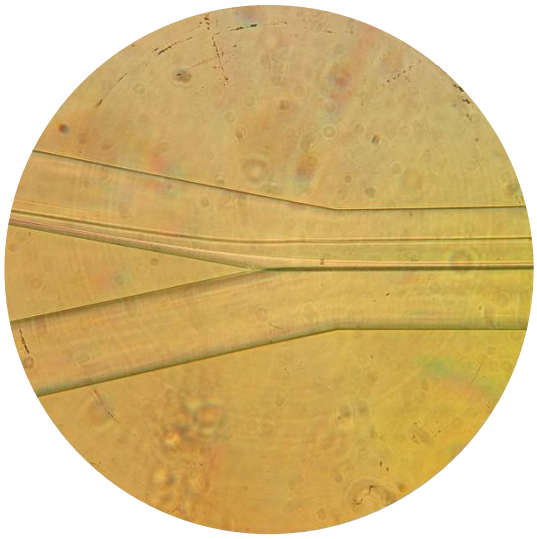

dichloromethane – 2.5% W

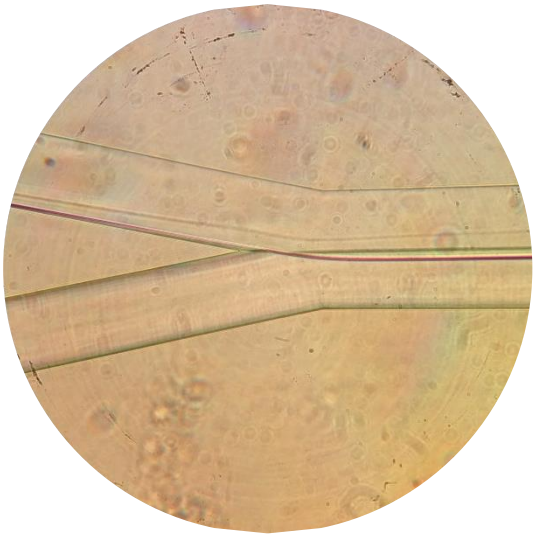

1,2-dichloroethane – 1% W

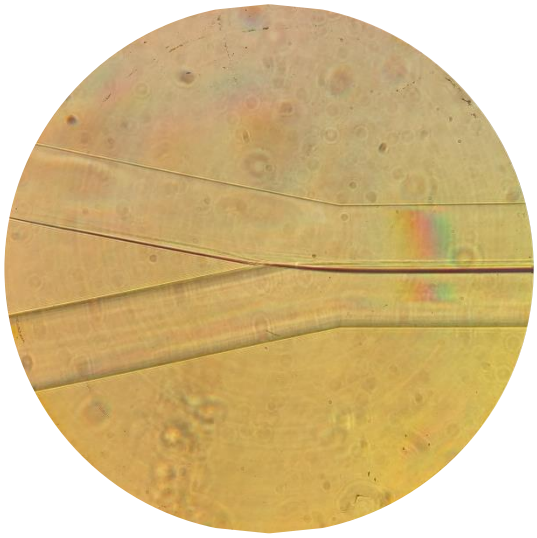

chloroform – 1% W

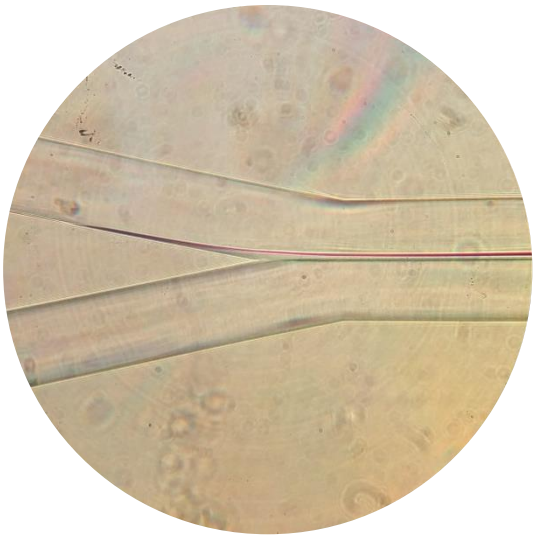

TBP – 0.5% W

TBP – 0.5% Mo

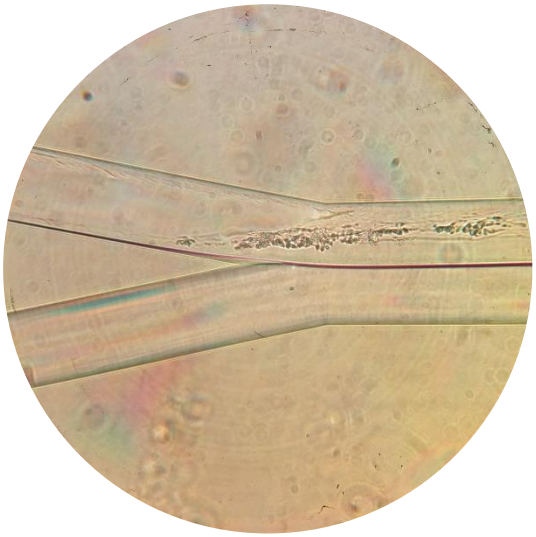

TBP – 1% W

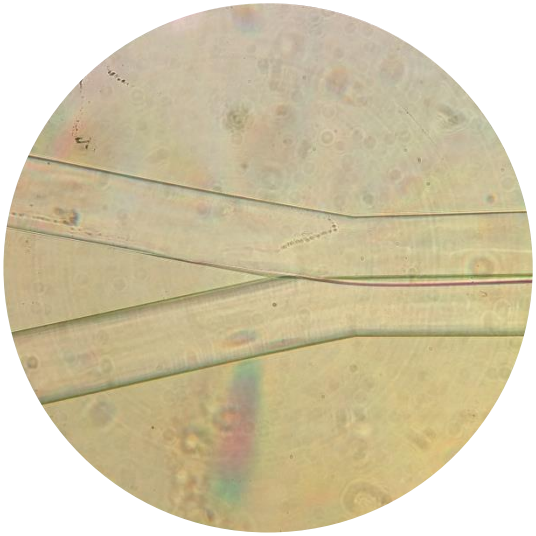

TBP – 1% Mo

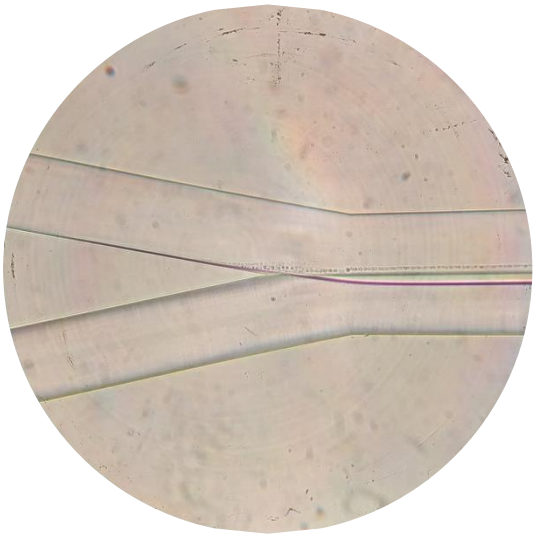

2-nonanone – 0.5% W

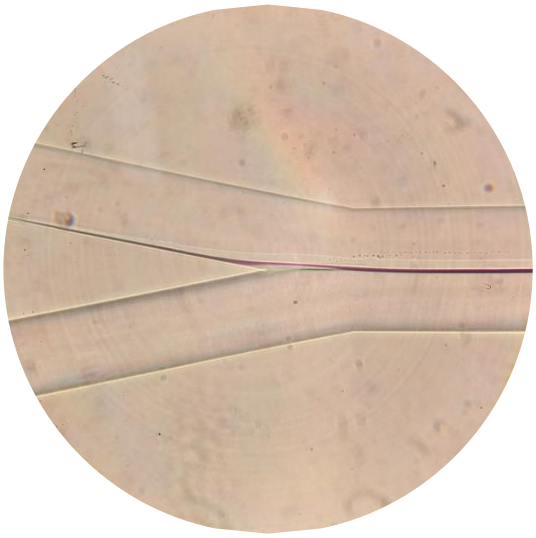

2-nonanone – 0.5% Mo

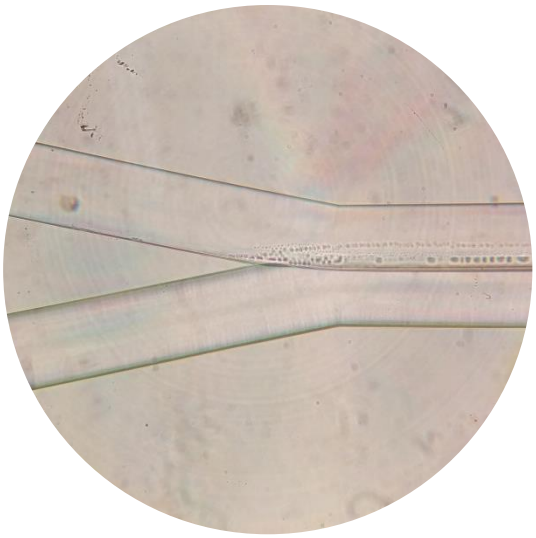

2-nonanone – 1% W

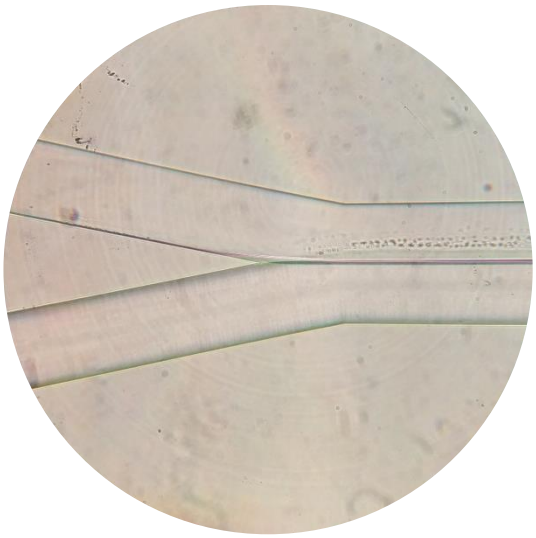

2-nonanone – 1% Mo

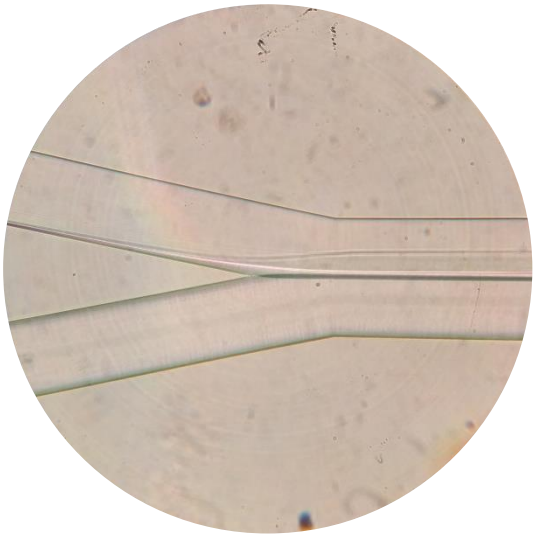

E06 – 2.5% W

9.2 Pictures aqueous infiltration

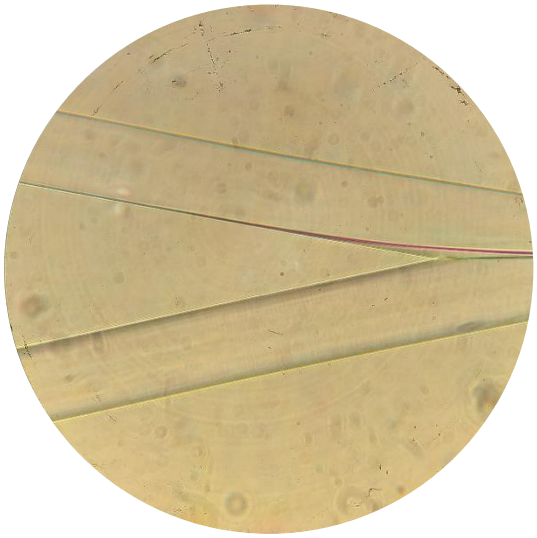

40 µl/min

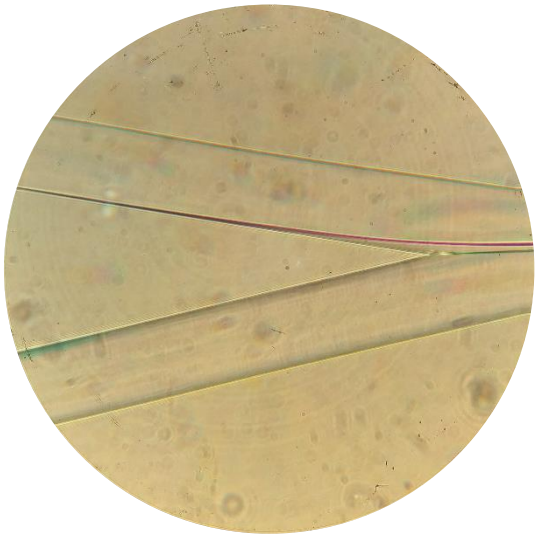

20 µl/min

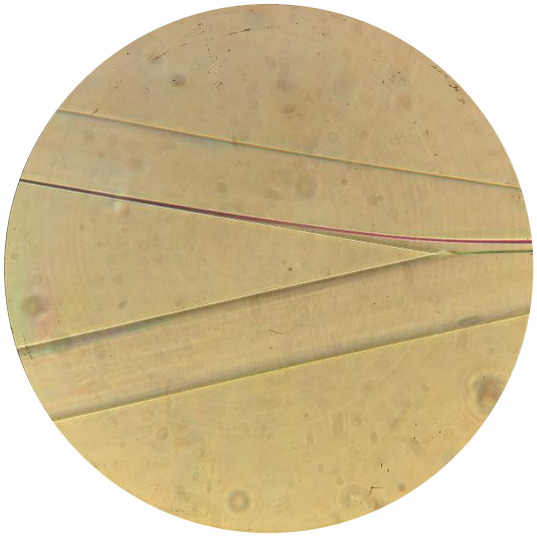

10 µl/min

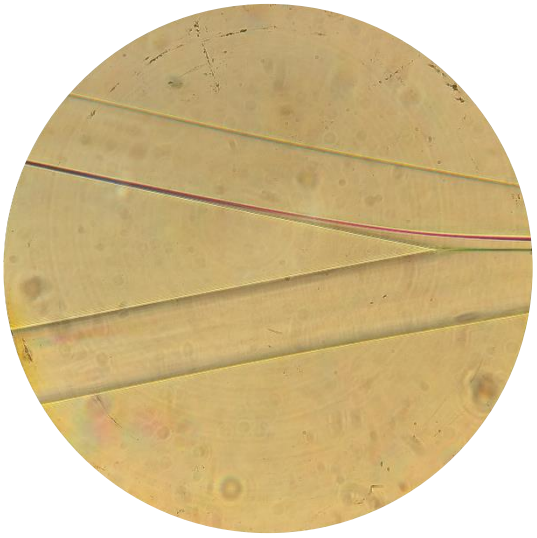

5 µl/min

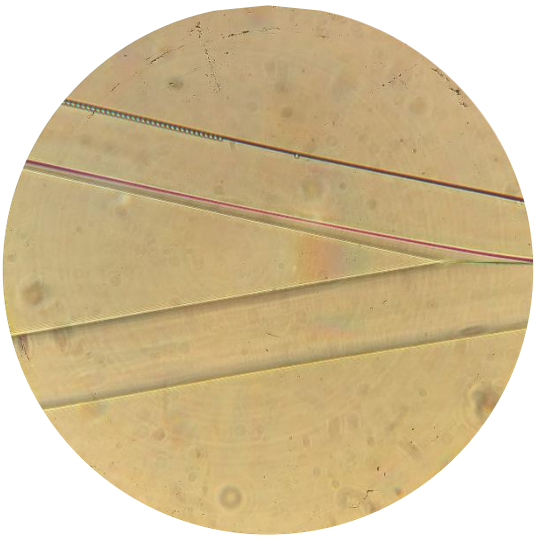

2.5 µl/min

9.3 Pictures simultaneous leakage

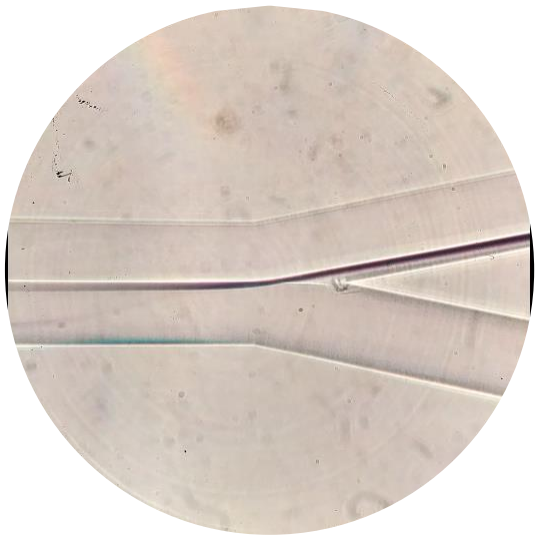
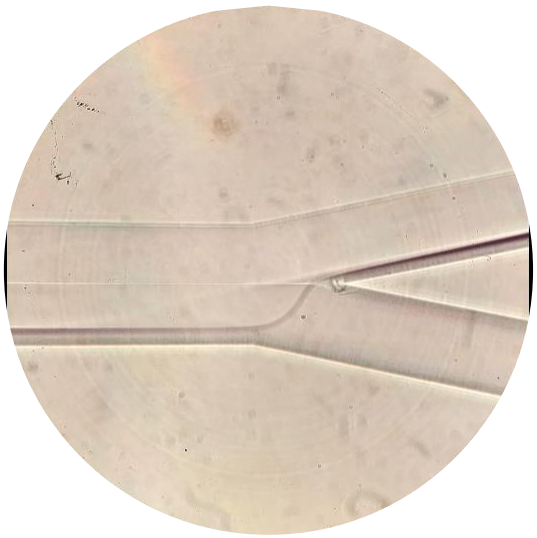
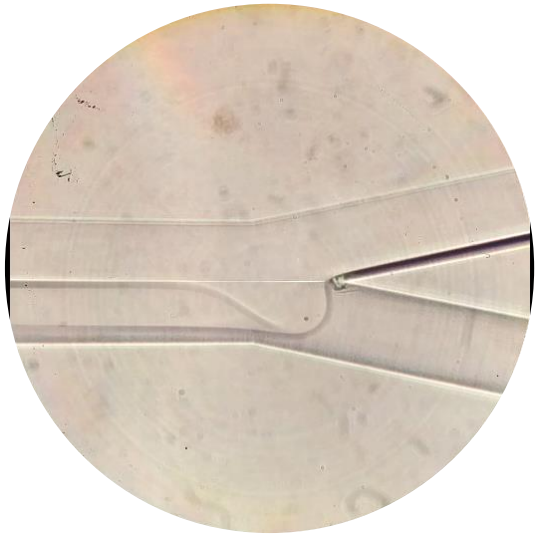
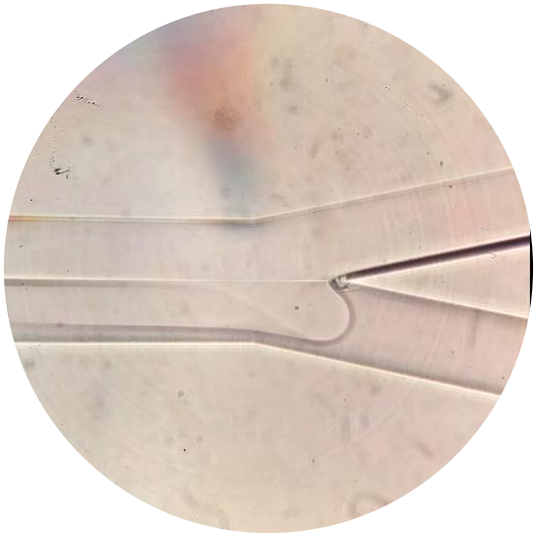
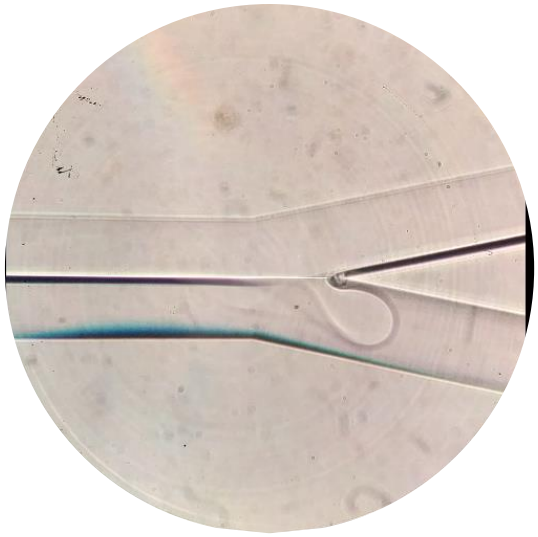
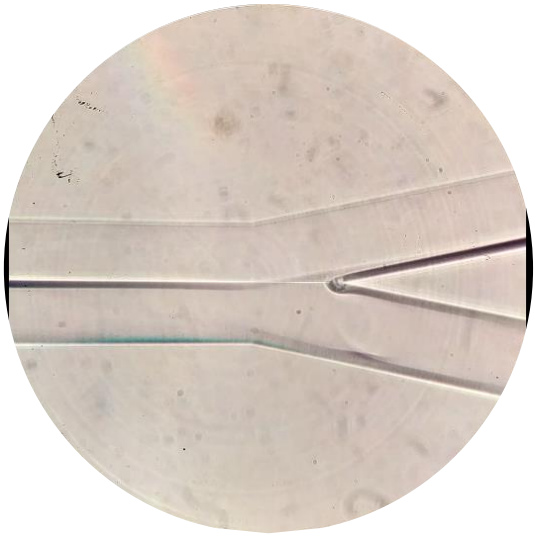

9.4 Activity calculations

BERAKT 1mg $NH_4ReO_4 \cdot 2H_2O$

stof	gewicht (mg)
H	1.51e-002
N	5.22e-002
O	2.39e-001
Re	6.94e-001

Faciliteit	ExtBefa1	
Bestralingstijd	11.00	minutes
Afkoeltijd	3.00	days
Dikte loodafscherming	0.045 m	

Direct na bestraling:

Totale radiotoxiciteit	2.22e-002 Sv
Dosistempo op 1 meter	4.30e-001 uSv/h
Dosistempo op 1 m met 0.045 m lood	6.12e-002 uSv/h
Opp. dosistempo op 10 cm	2.03e+004 uSv/h
Productnuclide	Re-188m

Na afkoeling:

Totale radiotoxiciteit	3.13e-003 Sv
Dosistempo op 1 meter	1.41e-002 uSv/h
Dosistempo op 1 m met 0.045 m lood	2.01e-003 uSv/h
Opp. dosistempo op 10 cm	4.07e+003 uSv/h
Productnuclide	Re-186

				(Gamma dosis)	(Gamma dosis)	(Beta dosis)
				(zonder lood)	(met lood)	
Target	Product	halfw.tijd	aktiviteit (Bq)	h10 (uSv/h)	h10 (uSv/h)	h07 (uSv/h)
Re-185	Re-186	3.78 d	1.66e+006	6.63e-003	9.44e-004	3.32e+003
Re-187	Re-186	3.78 d	2.50e+001	9.99e-008	1.42e-008	5.00e-002
Re-187	Re-188	16.98 h	7.50e+005	7.50e-003	1.07e-003	7.50e+002

BERAKT

1mg $Na_2WO4 \cdot 2H_2O$

stof	gewicht (mg)
H	1.22e-002
O	2.91e-001
Na	1.39e-001
W	5.57e-001

Faciliteit	ExtBefa1	
Bestralingstijd	7.50	minutes
Afkoeltijd	1.00	days
Dikte loodafscherming	0.045 m	

Direct na bestraling:

Totale radiotoxiciteit	1.32e-003 Sv
Dosistempo op 1 meter	1.96e-001 uSv/h
Dosistempo op 1 m met 0.045 m lood	2.78e-002 uSv/h
Opp. dosistempo op 10 cm	3.15e+003 uSv/h
Productnuclide	W-187

Na afkoeling:

Totale radiotoxiciteit	6.48e-004 Sv
Dosistempo op 1 meter	8.32e-002 uSv/h
Dosistempo op 1 m met 0.045 m lood	1.18e-002 uSv/h
Opp. dosistempo op 10 cm	1.54e+003 uSv/h
Productnuclide	W-187

				(Gamma dosis)	(Gamma dosis)	(Beta dosis)
				(zonder lood)	(met lood)	
Target	Product	halfw.tijd	aktiviteit (Bq)	h10 (uSv/h)	h10 (uSv/h)	h07 (uSv/h)
Na-23	Na-24	14.90 h	5.43e+004	2.75e-002	3.91e-003	5.43e+001
W-180	W-181	121.20 d	9.26e+000	8.34e-008	1.19e-008	6.48e-005
W-184	W-185	75.12 d	8.69e+002	8.69e-007	1.24e-007	8.69e-001
W-186	W-187	23.90 h	7.43e+005	5.57e-002	7.93e-003	1.49e+003

9.5 Dimensions IMT microchannel

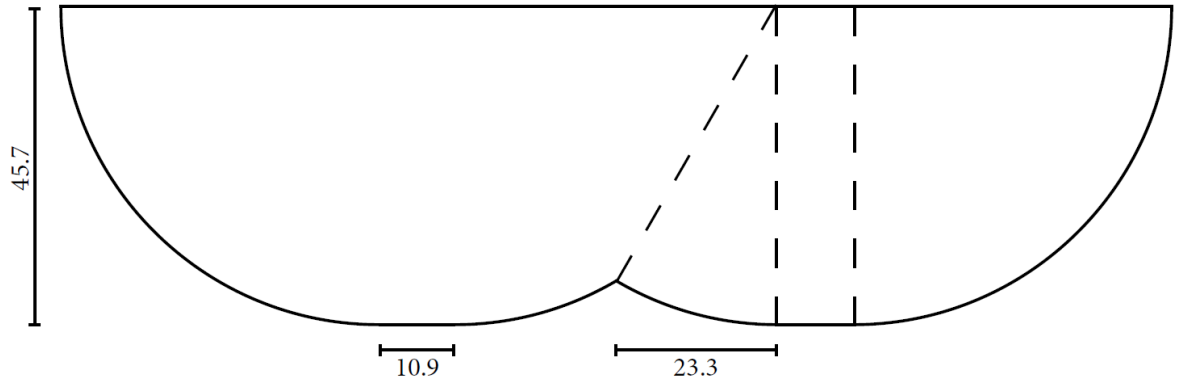

Figure 9-1. Schematic cross section of the main channel of the IMT chip. Numbers are micrometres. The drawing is to scale.

A schematic of the cross section of the main section is given in figure 9-1. The guide structure can be seen in the middle as a small peak. The total width of the channel is 160 µm and the height is roughly 46 µm. The dashed lines are solely there to divide the cross section in geometric shapes as to calculate cross-sectional area, which is 6.29E-9 m^2. The circumference of the cross-section is 3.73E-4 m and the hydraulic diameter (D_h) is then calculated to be 6.74E-5 m. The total length of the main channel with guide structure is 120 mm and he total volume of the main channel is 0.764 µl.

The lengths of the aqueous and organic inlet channel and aqueous and organic outlet channel are all 30 mm. These inlet and outlet channels also have a height of 46 µm but have widths of 100 µm. The cross-sectional area of the inlet and outlet channels is 3.78E-9 m^2. The circumference of the cross-section is 2.54E-04 m and the hydraulic diameter is then calculated to be 5.94E-5 m. The volume of each of the inlet or outlet channels is 0.113 µl.

The total volume of the microchannel plus inlet and outlet channels is therefore 1.2 µl.